EP2 AGONIST DID NOT INDUCE INFLAMMATION OF THE SYNOVIUM

It is important whether the EP2 agonist induced unfavorable inflammation during the regeneration process. We evaluated the synovium based on mRNA expression and histological scoring, and also measured the amounts of cytokines in joint fluid at 4 weeks. PGE2 was reported to up-regulate the expression of the *MMP3*, *TIMP3*, and *IL-1β* genes[3]. The expression of these inflammation-related genes was analyzed by semi-quantitative [Fig. 6(A)] and quantitative RT-PCR [Fig. 6(B)] using samples taken at 4 weeks. No significant up-regulation was found in either gene even in samples treated with a larger amount of EP2 agonist [Fig. 6(B)]. The activity of MMP3 in joint fluid had almost the same value as found in untreated joints [Fig. 6(C)]. The amount of TNF-α or CRP in treated knee joints showed no significant change compared with that in normal joints either [Fig. 6(D)]. Lining synovial cells showed no numerical or morphological change on treatment of with the agonist (400 μg/gel) [Fig. 6(E)], and the histological scoring for inflammation in the treated side was equal to that in the contralateral side [Fig. 6(F)]. These results

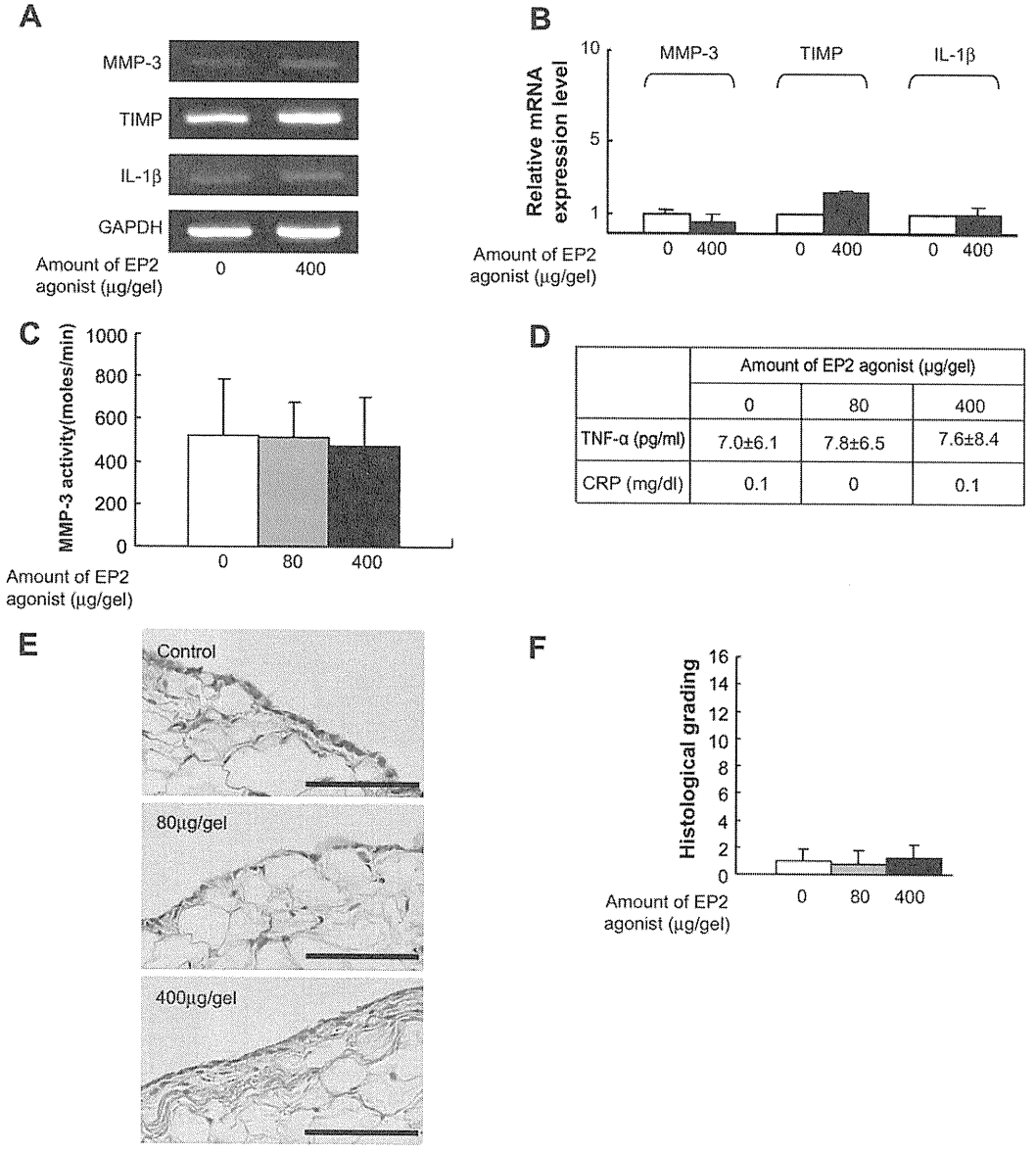

Fig. 6. EP2 agonist did not induce inflammation of the synovium. Inflammatory signs in knee joints were investigated in contralateral or EP2 agonist (80 or 400 μg/gel)-treated samples at 4 weeks after the operation in the osteochondral defect model. A and B: mRNA expression of inflammatory cytokines of cells in the synovium. RNA extracted from synovium was analyzed by semi-quantitative (A) and quantitative (B) RT-PCR. C: Activity of MMP3 in joint fluid. Joint fluid was collected from knee joints of contralateral (open square) and EP2 agonist-treated (blackened square) samples, and the activity of MMP3 was analyzed as described in the Materials and methods section. Five samples were analyzed in each group. D: Amount of TNF-α and CRP in joint fluid. Joint fluid was collected from five knee joints in each group. E: HE staining of synovium in knee joints. Specimens were prepared from a contralateral sample (a), and EP2 agonist-treated samples (b, 80 μg/gel; c, 400 μg/gel). Magnification 200×. Bar = 100 μm. F: Histological scoring of inflammation. Five specimens were analyzed in each of the contralateral and EP2 agonist-treated groups.

indicated that the EP2 agonist induced no significant inflammatory reaction in knee joints at the dose used in this study.

Discussion

PGE2 is a major prostanoid synthesized in response to various stimuli in a variety of cells and exerts local and systemic pleiotropic effects. In general, PGE2 plays a role in maintaining the physiological homeostasis, but in some pathogenic conditions such as inflammation and carcinogenesis, the excess PGE2 induced by factors such as inflammatory cytokines worsens the condition[10]. From this standpoint, PGE2 may be regarded as a pro-inflammatory factor promoting the pathological stage of OA. On the other hand, PGE2 has an anti-inflammatory function. Typical anti-inflammatory actions of PGE2 are demonstrated by the suppressive role of the PGE2 signal *via* EP3 in asthma[20]. As for the PGE2 signal *via* EP2, several reports have analyzed the relationship with inflammation. In human periodontal ligament cells, PGE2 signal *via* EP2/EP4 down-regulated the production of MMP3 and IL-6 stimulated by IL-1[21,22]. An EP4 agonist stimulated the production of MMP9 in macrophages, which was not observed on treatment with an EP2 agonist[23]. The expression of *COX-2* and *MMP9* genes was elevated in macrophages from EP2 null mice[24]. These results suggested that PGE2 acting through EP2 has a minimal role as a pro-inflammatory factor.

Our previous[11] and current study suggested that PGE2 signal *via* EP2 is not only anti-inflammatory but also promotes the regeneration of articular cartilage. The regeneration process of osteochondral defect may mimic the endochondral ossification in fracture healing, and several studies have already shown that the PGE2 signal involved in this process[25–28], among which signals *via* EP2 was particularly important[29]. Cells derived from bone marrow may play a central role in this process. On the other hand, the chondral defect model in this study may mimic the some stage of OA, in which cartilage tissue disappeared and subchondral bone was sclerosed. At this stage, the recruitment of bone marrow-derived cells was minimum, and, therefore, restoration of cartilage tissues was hardly observed. The therapeutic effects of EP2 agonist in this type of model, therefore, may be due to its effects directly on the remaining chondrocytes which are at the resting state in physiological condition as indicated by no PCNA staining [Fig. 3(A)]. The effects of EP2 agonist treatment were more prominent at the later time point (12 weeks) in both chondral and osteochondral defect models, suggesting that the regeneration of cartilage tissue was dependent on the growth of articular chondrocytes with low growth property. We observed that the amount of regenerated tissues was much less at 12 weeks than at 4 weeks after operation in control and contralateral samples, suggesting that regenerated cartilage tissues may lack the proper quality to maintain the structure, and the treatment with EP2 agonist may prevent such degeneration.

One of interesting finding in the current study is that the treatment with EP2 agonist enhanced the reconstruction of boundary between articular cartilage and subchondral bone, which is an important factor to maintain the articular structure. We have no clear explanation for this interesting phenomenon. As mentioned above, EP2 agonists stimulate the growth of both cartilage and bone marrow cells, which may relate to the physiological reconstruction of boundary.

It should be noted that the histological scale of contralateral samples tended to be better than that of control samples (Figs. 1 and 2) and the scales of contralateral samples of 400 μg/gel-treated animals were significantly better than 80 μg/gel-treated animals at 12 weeks [Fig. 2(D), $P = 0.02$], suggesting that there might be an effect from the treated-site through the systemic circulation. Although there were no signs of a general effect of PGE2 such as a reduction in blood pressure (data not shown), continuous release of the EP2 agonist may affect tissue regeneration on the contralateral side.

The ideal regeneration-promoting therapeutics will be small molecules which can be produced in a large amount, promote the regeneration of articular cartilage with a physiological structure, and have no adverse effects in other tissues either locally or systemically. No osteophyte formation was observed in any samples described in this study and also samples observed for a longer period (24 weeks) (data not shown). The results of this study suggested that the EP2 agonist is a promising candidate for such a new drug. Because EP4 is not expressed in normal articular chondrocytes[11], we have been focusing the analysis of EP2 agonist. In the case of osteochondral defect model, however, the combination of EP2/EP4 agonist is a reasonable choice to test considering the fact that the simultaneous activation of EP2 and EP4 cooperatively induced type II collagen mRNA expression[7]. The current experimental model has been used in several prior investigations of various articular repair procedures[30], but may not reflect the pathogenesis of OA (no mechanical factor, no inflammation, no aging factor). Further confirmation of the effect of EP2 agonists in combination with a more effective drug delivery system and experimental OA models in larger animals may lead to a new way to treat OA.

Conflict of interest

The authors declare that they have no conflict of interest.

Acknowledgments

We are grateful to Drs H. Ito, H. Yoshitomi, K. Nishitani, and B. Liang for providing helpful suggestions. This work was supported by Grants-in-aid for Scientific Research from the Japan Society for the Promotion of Science, from the Ministry of Education, Culture, Sports, Science, and Technology, and from the Ministry of Health, Labor, and Welfare.

Supplementary material

Supplementary material for this article may be found, in the online version, at doi: 10.1016/j.joca.2008.09.003.

References

1. Goldring MB, Goldring SR. Osteoarthritis. J Cell Physiol 2007;213: 626–34.
2. Goldring SR, Goldring MB. The role of cytokines in cartilage matrix degeneration in osteoarthritis. Clin Orthop Relat Res 2004;(427 Suppl):S27–36.
3. Martel-Pelletier J, Pelletier JP, Fahmi H. Cyclooxygenase-2 and prostaglandins in articular tissues. Semin Arthritis Rheum 2003;33:155–67.
4. Bunning RA, Russell RG. The effect of tumor necrosis factor alpha and gamma-interferon on the resorption of human articular cartilage and on the production of prostaglandin E and of caseinase activity by human articular chondrocytes. Arthritis Rheum 1989;32:780–4.
5. Miwa M, Saura R, Hirata S, Hayashi Y, Mizuno K, Itoh H. Induction of apoptosis in bovine articular chondrocyte by prostaglandin E(2) through cAMP-dependent pathway. Osteoarthritis Cartilage 2000;8: 17–24.

6. Riquet FB, Lai WF, Birkhead JR, Suen LF, Karsenty G, Goldring MB. Suppression of type I collagen gene expression by prostaglandins in fibroblasts is mediated at the transcriptional level. Mol Med 2000;6:705–19.
7. Miyamoto M, Ito H, Mukai S, Kobayashi T, Yamamoto H, Kobayashi M, *et al.* Simultaneous stimulation of EP2 and EP4 is essential to the effect of prostaglandin E2 in chondrocyte differentiation. Osteoarthritis Cartilage 2003;11:644–52.
8. Di Battista JA, Doré S, Morin N, He Y, Pelletier JP, Martel-Pelletier J. Prostaglandin E2 stimulates insulin-like growth factor binding protein-4 expression and synthesis in cultured human articular chondrocytes: possible mediation by Ca(++)-calmodulin regulated processes. J Cell Biochem 1997;65:408–19.
9. Lowe GN, Fu YH, McDougall S, Polendo R, Williams A, Benya PD, *et al.* Effects of prostaglandins on deoxyribonucleic acid and aggrecan synthesis in the RCJ 3.1C5.18 chondrocyte cell line: role of second messengers. Endocrinology 1996;137:2208–16.
10. Sugimoto Y, Narumiya S. Prostaglandin E receptors. J Biol Chem 2007; 282:11613–7.
11. Aoyama T, Liang B, Okamoto T, Matsusaki T, Nishijo K, Ishibe T, *et al.* PGE2 signal through EP2 promotes the growth of articular chondrocytes. J Bone Miner Res 2005;20:377–89.
12. Tani K, Naganawa A, Ishida A, Egashira H, Sagawa K, Harada H, *et al.* Design and synthesis of a highly selective EP2-receptor agonist. Bioorg Med Chem Lett 2001;11:2025–8.
13. Okada H. One- and three-month release injectable microspheres of the LH–RH superagonist leuprorelin acetate. Adv Drug Deliv Rev 1997; 28:43–70.
14. Katayama R, Wakitani S, Tsumaki N, Morita Y, Matsushita I, Gejo R, *et al.* Repair of articular cartilage defects in rabbits using CDMP1 gene-transfected autologous mesenchymal cells derived from bone marrow. Rheumatology (Oxford) 2004;43:980–5.
15. Yoshimi T, Kikuchi T, Obara T, Yamaguchi T, Sakakibara Y, Itoh H, *et al.* Effects of high-molecular-weight sodium hyaluronate on experimental osteoarthrosis induced by the resection of rabbit anterior cruciate ligament. Clin Orthop Relat Res 1994;298:296–304.
16. Fukuda T, Tani Y, Kobayashi T, Hirayama Y, Hino O. A new Western blotting method using polymer immunocomplexes: detection of Tsc1 and Tsc2 expression in various cultured cell lines. Anal Biochem 2000;285:274–6.
17. Qi C, Changlin H, Zefeng H. Matrix metalloproteinases and inhibitor in knee synovial fluid as cartilage biomarkers in rabbits: the effect of high-intensity jumping exercise. J Surg Res 2007;140:149–57.
18. Wu LD, Yu HC, Xiong Y, Feng J. Effect of dehydroepiandrosterone on cartilage and synovium of knee joints with osteoarthritis in rabbits. Rheumatol Int 2006;27:79–85.
19. Kawashima-Ohya Y, Satakeda H, Kuruta Y, Kawamoto T, Yan W, Akagawa Y, *et al.* Effects of parathyroid hormone (PTH) and PTH-related peptide on expressions of matrix metalloproteinase-2, -3, and -9 in growth plate chondrocyte cultures. Endocrinology 1998;139:2120–7.
20. Kunikata T, Yamane H, Segi E, Matsuoka T, Sugimoto Y, Tanaka S, *et al.* Suppression of allergic inflammation by the prostaglandin E receptor subtype EP3. Nat Immunol 2005;6:524–31.
21. Yan M, Noguchi K, Ruwanpura SM, Ishikawa I. Cyclooxygenase-2-dependent prostaglandin (PG) E2 downregulates matrix metalloproteinase-3 production *via* EP2/EP4 subtypes of PGE2 receptors in human periodontal ligament cells stimulated with interleukin-1alpha. J Periodontol 2005;76:929–35.
22. Noguchi K, Maeda M, Ruwanpura SM, Ishikawa I. Prostaglandin E2 (PGE2) downregulates interleukin (IL)-1alpha-induced IL-6 production *via* EP2/EP4 subtypes of PGE2 receptors in human periodontal ligament cells. Oral Dis 2005;11:157–62.
23. Tchetina EV, Di Battista JA, Zukor DJ, Antoniou J, Poole AR. Prostaglandin PGE2 at very low concentrations suppresses collagen cleavage in cultured human osteoarthritic articular cartilage: this involves a decrease in expression of proinflammatory genes, collagenases and COL10A1, a gene linked to chondrocyte hypertrophy. Arthritis Res Ther 2007;9:R75.
24. Pavlovic S, Du B, Sakamoto K, Khan KM, Natarajan C, Breyer RM, *et al.* Targeting prostaglandin E2 receptors as an alternative strategy to block cyclooxygenase-2-dependent extracellular matrix-induced matrix metalloproteinase-9 expression by macrophages. J Biol Chem 2006;281:3321–8.
25. Simon AM, Manigrasso MB, O'Connor JP. Cyclo-oxygenase 2 function is essential for bone fracture healing. J Bone Miner Res 2002;17: 963–76.
26. Gerstenfeld LC, Al-Ghawas M, Alkhiary YM, Cullinane DM, Krall EA, Fitch JL, *et al.* Selective and nonselective cyclooxygenase-2 inhibitors and experimental fracture-healing. Reversibility of effects after short-term treatment. J Bone Joint Surg Am 2007;89:114–25.
27. Einhorn TA. The science of fracture healing. J Orthop Trauma 2005; 19(10 Suppl):S4–6.
28. Yamakawa K, Kamekura S, Kawamura N, Saegusa M, Kamei D, Murakami M, *et al.* Association of microsomal prostaglandin E synthase 1 deficiency with impaired fracture healing, but not with bone loss or osteoarthritis, in mouse models of skeletal disorders. Arthritis Rheum 2008;58:172–83.
29. Paralkar VM, Borovecki F, Ke HZ, Cameron KO, Lefker B, Grasser WA, *et al.* An EP2 receptor-selective prostaglandin E2 agonist induces bone healing. Proc Natl Acad Sci U S A 2003; 100:6736–40.
30. Breinan HA, Hsu HP, Spector M. Chondral defects in animal models: effects of selected repair procedures in canines. Clin Orthop Relat Res 2001;(391 Suppl):S219–30.

TISSUE ENGINEERING: Part C
Volume 16, Number 1, 2010

DOI: 10.1089/ten.tec.2008.0693

A Novel Method to Isolate Mesenchymal Stem Cells from Bone Marrow in a Closed System Using a Device Made by Nonwoven Fabric

Kinya Ito, M.D.,[1,2] Tomoki Aoyama, M.D., Ph.D.,[1] Kenichi Fukiage, M.D.,[1,3] Seiji Otsuka, M.D., Ph.D.,[1,2] Moritoshi Furu, M.D.,[1,3] Yonghui Jin, M.D.,[1] Akira Nasu, M.D.,[1,3] Michiko Ueda,[1] Yasunari Kasai,[4] Eishi Ashihara, M.D., Ph.D.,[4] Shinya Kimura, M.D., Ph.D.,[4] Taira Maekawa, M.D., Ph.D.,[4] Akira Kobayashi, Ph.D.,[5] Shinya Yoshida, Ph.D.,[5] Hideo Niwa, Ph.D.,[5] Takanobu Otsuka, M.D., Ph.D.,[2] Takashi Nakamura, M.D., Ph.D.,[3] and Junya Toguchida, M.D., Ph.D.[1]

Bone marrow stromal cells (BMSCs) include cells with multidirectional differentiation potential described as mesenchymal stem cells. For clinical use, it is important to develop a way to isolate BMSCs from bone marrow in a closed system without centrifugation. After screening 200 biomaterials, we developed a device containing a nonwoven fabric filter composed of rayon and polyethylene. The filter selectively traps BMSCs among mononuclear cells in bone marrow based on affinity, not cell size. The cells are then recovered by the retrograde flow. Using canine and human bone marrow cells, the biological properties of BMSCs isolated by the device were compared with those obtained by conventional methods using centrifugation. The total number isolated by the device was larger, as was the number of $CD106^+/STRO\text{-}1^+$ double-positive cells. The cells showed osteogenic, chondrogenic, and adipogenic differentiation potential *in vitro*. Finally, the direct transplantation of cells isolated by the device without *in vitro* cultivation accelerated bone regeneration in a canine model of osteonecrosis *in vivo*. The proposed method is rapid and efficient, does not require a biological clean area, and will be useful for the clinical application of mesenchymal stem cells in bone marrow.

Introduction

Bone marrow stromal cells (BMSCs) include cells with multidirectional differentiation potential such as mesenchymal stem cells (MSCs), multipotent adult progenitor cells, and marrow-isolated adult multilineage inducible cells, although it is not yet clear whether these cell types are distinct or overlap.[1,2] In spite of such ambiguity, BMSC-derived multipotent cells have been used in various fields of regenerative medicine. For clinical applications, however, it is critical to develop a method separating BMSCs containing multipotent cells from other types of cells in bone marrow that is simple, safe, inexpensive, and achievable in a closed system. The most popular way to isolate BMSCs is the density gradient method using a detergent such as sucrose[3] although the process is technically demanding and time consuming. Simple centrifugation with low gravity can also separate mononuclear cells (MNCs) from erythrocytes, and BMSCs can be selected through adherence to plastic dishes.[4] This method, however, still needs centrifugation, which makes it difficult to perform in a closed system, and therefore requires a biologically clean room.

To avoid the need for centrifugation, we have attempted to develop a device that can isolate BMSCs by filtration, and have selected nonwoven fabrics as biomaterials. Nonwoven fabrics are engineered materials that provide specific functions such as absorbency, liquid repellency, resilience, stretch, softness, strength, flame retardancy, washability, and cushioning.[5] As for clinical applications, nonwoven fabrics are used mainly for two purposes, as scaffolds and filters. A number of studies have used nonwoven fabrics as scaffolds for tissue regeneration.[5–7] The material and diameter of the fabric are important for cell attachment.[6,8] For example, polyethylene terephthalate with fibers 9.0 μm in diameter is ideal for the osteogenic differentiation of MSCs.[6] As filters, nonwoven fabrics have been used to sterilize medical materials.[9] Lymphocytapheresis is a form of treatment for patients with autoimmune diseases, in which lymphocytes in

[1]Institute for Frontier Medical Sciences, Kyoto University, Kyoto, Japan.
[2]Department of Orthopaedic Surgery, Graduate School of Medical Sciences, Nagoya City University, Nagoya, Japan.
[3]Department of Orthopaedic Surgery, Graduate School of Medicine, Kyoto University, Kyoto, Japan.
[4]Department of Transfusion Medicine and Cell Therapy, Kyoto University Hospital, Kyoto, Japan.
[5]Kaneka Co., Osaka, Japan.

peripheral blood are removed to reduce immunoreactions. To replace the centrifugation process in lymphocytapheresis, a filtration method using nonwoven fabrics has been developed.[10] The trapping effect is attributed to the affinity of the material for cells and the size of the material's fibers, with almost all leukocytes trapped when the fibers are less than 3 μm in diameter.[10,11]

As pure mechanical trapping based on cell size can damage cell membranes, we have tried to develop a filter that traps MSCs through affinity and here show that a new device composed of rayon–polyethylene nonwoven fabrics can isolate BMSCs from bone marrow aspirates, which contain cells compatible with multipotent cells *in vitro* and *in vivo*.

Materials and Methods

Screening of materials

The basic concept behind our approach is to trap BMSCs among bone marrow aspirates on a filter, and collect them using a retrograde flow (Fig. 1A). Biomaterials for the filter were screened based on microscopic structure (evenness), diameter (over 10 μm), weight (over 50 g/m^2), bio-safety, and availability (as the first screening). Potentially suitable biomaterials were further screened by conducting colony-forming unit (CFU) assays described later using swine bone marrow cells in three steps (as the second, third, and fourth screening; Supplemental Fig. S1, available online at www.liebertonline.com).

Electron microscopic analyses

After bone marrow had permeated through it, the filter was treated with 2.5 wt% glutaraldehyde in saline for 2 days at 4°C. The samples were dried by passing them through a series of graded-alcohol-saline solutions. Finally, the solution was changed to 100% t-butanol, and the samples were freeze-dried for 10 h at −5°C. The dried membranes were coated with gold–palladium and examined using a S-3000N scanning electron microscope (Hitachi, Tokyo, Japan).

Harvesting of bone marrow

Humans. Ten milliliters of bone marrow was taken from iliac crests of donors who received orthopedic operative procedures requiring autologous bone grafts from iliac crests. The donors had no history of concurrent illness or of medication that could affect bone metabolism. The Ethics Committee of the Faculty of Medicine, Kyoto University, approved the procedure, and informed consent was obtained from each donor according to the declaration of Helsinki.

Dogs. Ten milliliters of bone marrow was aspirated from iliac crests of male beagle dogs (10–13 kg) under intravenous anesthesia. The experiments with animals were approved by the institutional animal research committee, and performed according to the Guidelines for Animal Experiments of Kyoto University.

Preparation of MNCs

Human marrow samples were divided equally into three aliquots (3 mL each). One aliquot was applied to the device (method D), which had been saturated with saline. After washing the filter with 10 mL of saline, trapped cells were collected by a retrograde flow of the culture medium into a collection bag (Fig. 1A). The second aliquot was suspended in 5 mL of α-minimum essential medium GlutaMAX (Invitrogen, Carlsbad CA,) with 10% fetal bovine serum (Hyclone, South Logan, UT). The suspension was centrifuged at 1200 rpm for 5 min. The supernatant and the buffy coat were re-suspended in another tube with 5 mL of α-minimum essential medium GlutaMAX with 10% fetal bovine serum. This method is hereafter designated method S (simple centrifugation).[4,12] The final aliquot of bone marrow was fractionated by centrifugation over a density cushion using a Ficoll gradient (GE Healthcare Life Sciences, Piscataway, NJ), as described.[3] The interface layer was harvested and washed twice with 10 mL of Hank's buffer solution. This method is hereafter designated method F (Ficoll gradient).

Collection efficacy

Cells trapped on the filter and collected by retrograde flow in the collection bag were designated the collected fraction, and cells flowing through the filter into the flow-through bag were designated the flow-through fraction (Fig. 1A). Collection efficacy was determined as the ratio of the number of cells in each fraction to that in the applied bone marrow.

CFU assay

For the CFU assay, the MNCs were diluted and plated in 60-mm cell culture dishes at a density of 2.5×10^5 cells/dish and incubated for 14 days ($n=3$). The cells were fixed with methanol and stained with a 0.05% crystal violet solution. We counted the number of colony with a diameter more than 4 mm.

Flow cytometry

Cells were stained at room temperature for 30 min with the following antibodies: CD10-phycoerythrin (PE), CD34-allophycocyanin (APC), CD45-peridinin chlorophyll protein (PerCP-Cy5.5), CD106-fluorescein isothiocyanate (FITC), CD166-PE (BD Biosciences, San Jose, CA), CD90-FITC (Beckman Coulter, Fullerton, CA), CD271-APC (Miltenyi Biotec, Bergisch Gladbach, Germany), and STRO-1-PE (Santa Cruz Biotechnology, Santa Cruz, CA). They were subsequently subjected to flow cytometry using a FACS Calibur instrument (BD Biosciences).

Induction of differentiation and histochemical evaluating

Differentiation was induced using the standard method.[13] The differentiation potential was evaluated as below.

- Osteogenic differentiation: Calcified nodules were evaluated by alizarin red staining, and calcium content was quantified.
- Adipogenic differentiation: Intracellular lipid droplets were stained with oil red-O, and the amount of triglyceride was quantified.
- Chondrogenic differentiation: Cartilage matrix was evaluated by alcian blue staining, and the amount of glycosaminoglycan was quantified.

These analyses were described previously.[14]

Reverse transcription–polymerase chain reaction

Total RNA was extracted using RNeasy Kit (Qiagen, Hilden, Germany). All reverse transcription reactions were

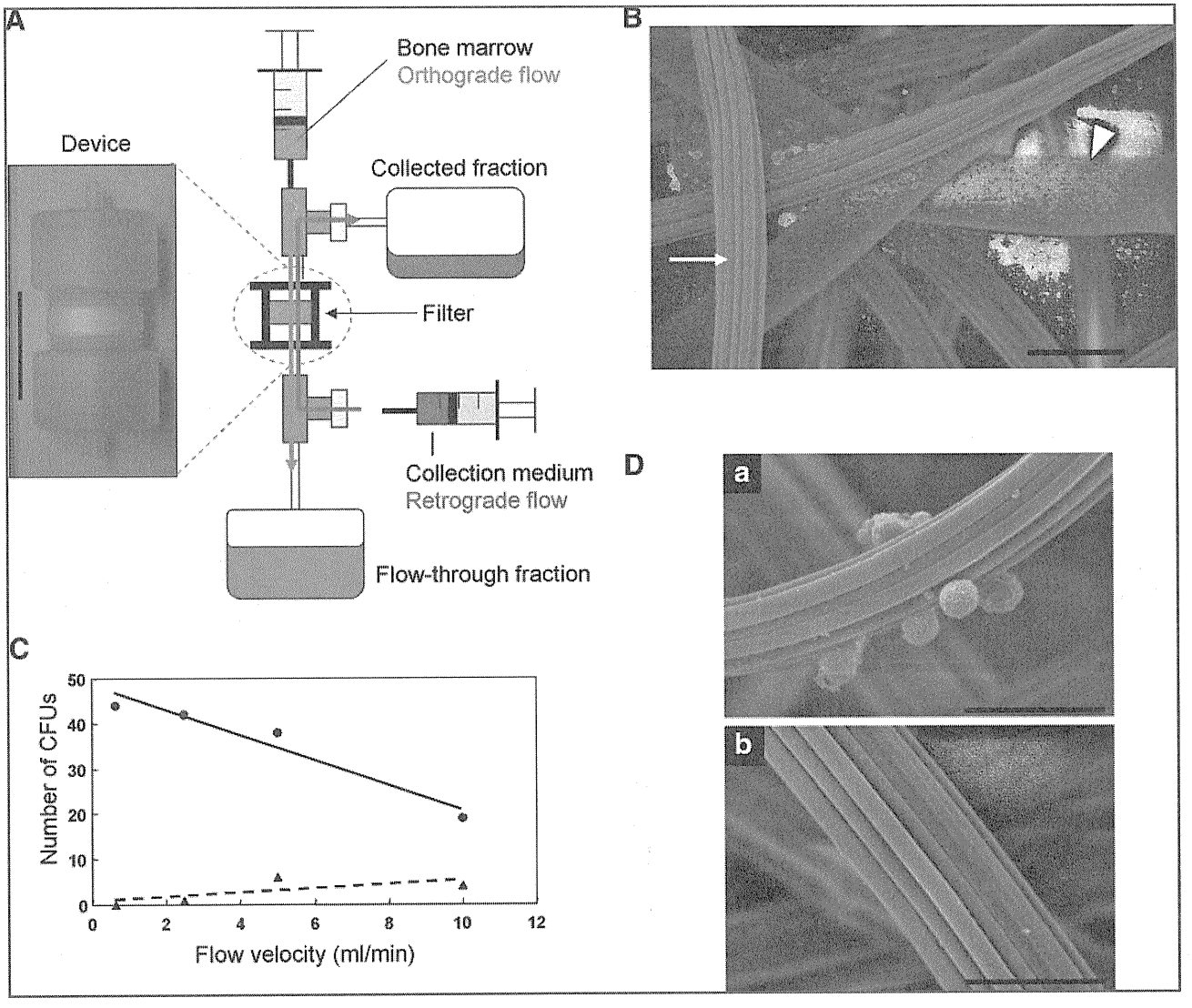

FIG. 1. Device containing a nonwoven fabric filter. (**A**) Photo of the device and schematic explanation of the collection method. The red line indicates the orthograde flow to apply bone marrow, and the blue line indicates the retrograde flow to collect cells. Scale bar = 30 mm. (**B**) Electron micrograph of the nonwoven fabric of rayon and polyethylene. Arrow, rayon; arrowhead, polyethylene. Magnification, 2000×. Scale bar = 20 μm. (**C**) Conditioning of flow velocity using swine bone marrow. Closed circles and closed triangles indicate the number of colony-forming units (CFUs) formed by cells in the collected fraction and flow-through fraction at the indicated flow velocity, respectively. (**D**) Electron micrograph of the surface of the filter after the orthograde flow of swine bone marrow (a) and after the retrograde flow of collection medium (b). Magnification, 2500×. Scale bar = 20 μm.

performed using the Super Script First Strand Synthesis System (Invitrogen). Polymerase chain reaction amplification was carried out using rTaq polymerase (Toyobo, Osaka, Japan). All polymerase chain reactions were performed using GeneAmp 9700 (PE Applied Biosystem, Foster City, CA) and specific primers for each gene.[14]

Preparation of the canine model of osteonecrosis and cell transplantation

A canine model of scapho-lunate osteonecrosis was prepared as described previously.[15] Briefly, scapho-lunates on one side were exposed dorsally, and a cortical window of 5×10 mm was made, through which as much cancerous bone as possible was removed. After the curettage, the cavity was filled with liquid nitrogen for 10 min, and the frozen bone was thawed at room temperature for 10 min. This freeze–thaw procedure was repeated three times. On one side, the bone cavity was filled with beta-tricalcium phosphate (β-TCP) granules (200 μg, 0.2 cm^3) (Osferion®; Olympus, Tokyo, Japan) (hereafter designated the control side). On the other side, canine BMSCs ($6.0\times10^7 \pm 1.5\times10^7$) isolated by the device from 10 mL of bone marrow were mixed with the same amount of β-TCP and transplanted into the bone cavity (hereafter designated the BMSC side). Finally, the bone window was plugged with 5×10 mm cortical bone. Animals were sacrificed and evaluated at 4 weeks after the operation ($n = 6$).

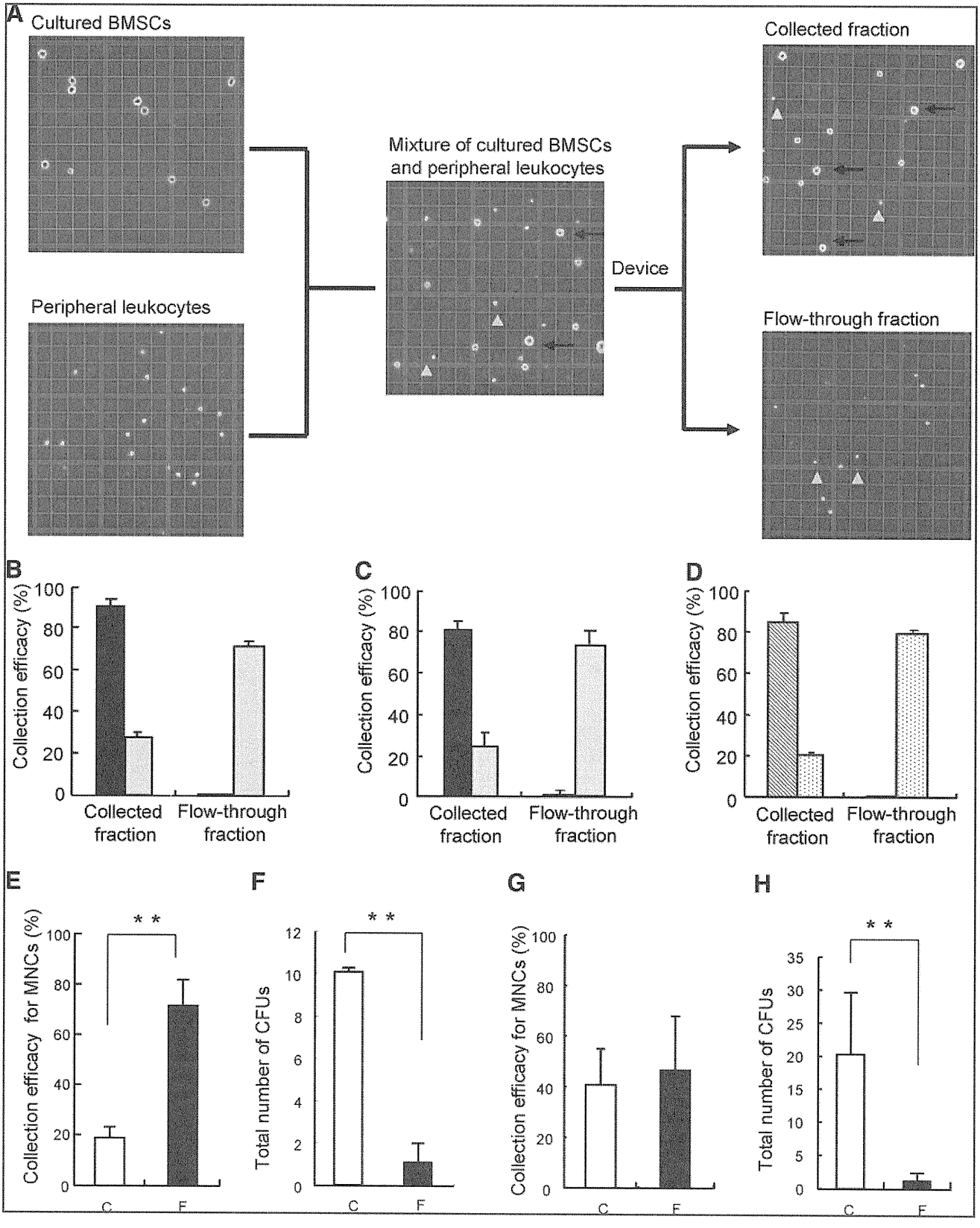
A
Cultured BMSCs
Peripheral leukocytes
Mixture of cultured BMSCs and peripheral leukocytes
Device
Collected fraction
Flow-through fraction
B
C
D
Collection efficacy (%)
Collected fraction
Flow-through fraction
E
F
G
H
Collection efficacy for MNCs (%)
Total number of CFUs
* *
C
F

Imaging analyses

X-ray. Antero-posterior and lateral views of both wrists were obtained. The carpal height ratio was calculated from the antero-posterior view.[15,16] The Ståhl index was calculated from the lateral view.[15,17]

Micro-computed tomography. Canine carpal bones were scanned by computed tomography (CT) (SMX-100CT-SV3 type; Shimazu, Kyoto, Japan). The image consisted of 800 slices with a voxel size of 68.224 mm in all three axes. Coronal and sagittal cross-sectional views of the scapho-lunate were reconstructed using adjunctive software. The same setting was used for all samples. The image reconstruction and quantification of the scapho-lunate were performed with VG Studio MAX software (Nihon Visual Science, Tokyo, Japan).[15]

Macroscopic and microscopic assessments

The volume and weight of extracted scapho-lunate bones were actually measured using a scale. The samples were fixed in a 10% formalin solution, decalcified with Plank-Rychlo solution, and then embedded in paraffin. Serial sections were cut at 4 μm, and stained with hematoxylin–eosin and silver impregnation.

Using a light microscope, the absorption of β-TCP granules and the formation of bone were graded as follows.[18] For hematoxylin–eosin staining, granules were not surrounded by cells or newly forming bone (grade 1); granules were surrounded by osteoblasts and/or osteoclasts (grade 2); and granules were surrounded by newly forming bone (grade 3). For silver impregnation staining, granules were not completely surrounded by collagen fibrils (grade 1); granules were completely surrounded by collagen fibrils (grade 2); and granules were completely eroded with reticulated collagen fibrils (grade 3). All the β-TCP granules in a whole section were classified according to the three grades. The rates of each grade were then calculated.

Statistics

Results are expressed as the mean ± SE. The statistical analysis was first performed by the analysis of variance (ANOVA), and if there was a significant difference among samples, Turkey's *post hoc* test was performed for multiple comparisons. The Student's *t*-test was carried out to compare individual data. A significant difference was accepted at $p < 0.05$.

Results

Screening of materials

The first screening, of 200 potential biomaterials for the filter, was based on the parameters described in the Materials and Methods section. Forty materials were then selected for the second screening using swine bone marrow cells ($n = 2$). Ten biomaterials showed CFU counts of more than 10, and were selected for the third screening by CFU assay ($n = 3$), of which six preceded to the fourth and last screening ($n = 3$). Finally, a rayon–polyethylene nonwoven fabric was selected as the material for the filter (Supplemental Fig. S1, available online at www.liebertonline.com). First, the optimum velocity of filtration was determined by comparing CFU counts of cells in the collected and flow-through fractions. A velocity of 2.5 mL/min was chosen for further experiments (Fig. 1C). Electron microscopic analysis confirmed the binding of swine bone marrow cells and their detachment under retrograde flow (Fig. 1D, a and b).

Selective collection of BMSCs by the device

To analyze the device's selectivity, cultured human BMSCs or peripheral leukocytes were applied to it, and the cells in the collected fraction and flow-through fractions were enumerated (Fig. 2B). More than 90% of BMSCs were collected in the collected fraction, compared to only 28% of peripheral leukocytes (Fig. 2B). This selectivity was also observed when equal numbers (1×10^6) of BMSCs and peripheral leukocytes were mixed and then applied to the device (Fig. 2C). Because BMSCs and peripheral leukocytes differ in size, we could distinguish between them in the cell counting chamber (Fig. 2A). Approximately 80% of BMSCs were collected in the collected fraction, and an almost equal percentage of peripheral leukocytes were collected in the flow-through fraction (Fig. 2C). More than 90% of $CD44^+$ cells were collected with the device, leaving almost no $CD44^+$ cells in the flow-through fraction, whereas less than 20% of $CD45^+$ cells were collected (Fig. 2D). These results suggested the selective collection of BMSCs by the device.

FIG. 2. Selective collection of bone marrow stromal cells (BMSCs) with CFUs by the device. (**A**) Selective counting of BMSCs and peripheral leukocytes. BMSCs and peripheral leukocytes differed in morphology in the cell counting chamber (left two photos). After the mixing of the two types of cells (middle) and application of the device, each type of cell in the collected (right upper) or flow-through (right lower) fraction was numerated. Arrow, cultured BMSCs; arrowhead, peripheral leukocytes. (**B**) Collection efficacy for human BMSCs (black box) and peripheral leukocytes (gray box). Each type of cell was applied to the device separately, and collection efficacy was calculated from the number of cells in the collected and flow-through fractions. (**C**) Collection efficacy for human BMSCs (black box) and peripheral leukocytes (gray box). Equal numbers of BMSCs and peripheral leukocytes were mixed and applied to the device. Collection efficacy was calculated from the number of cells in the collected and flow-through fractions. (**D**) Collection efficacy for CD44 (hatched box) and $CD45^+$ (dotted box) cells. Equal numbers of BMSCs and peripheral leukocytes were mixed and applied to the device. Cells positive for CD44 or CD45 in the collected or flow-through fraction were numerated by fluorescence-activated cell sorting (FACS), and collection efficacy was calculated from the number of positive cells in the cell mixture before the treatment. (**E**) Collection efficacy for mononuclear cells (MNCs) from canine bone marrow. $^{**}p < 0.01$ (**F**) Total number of CFUs derived from canine MNCs collected in the collected and flow-through fractions. From the results on collection efficacy and number of CFUs, the total number of CFUs was calculated. $^{**}p < 0.01$. (**G**) Collection efficacy for MNCs from human bone marrow. (**H**) Total number of CFUs derived from human MNCs collected in the collected and flow-through fractions. $^{**}p < 0.01$.

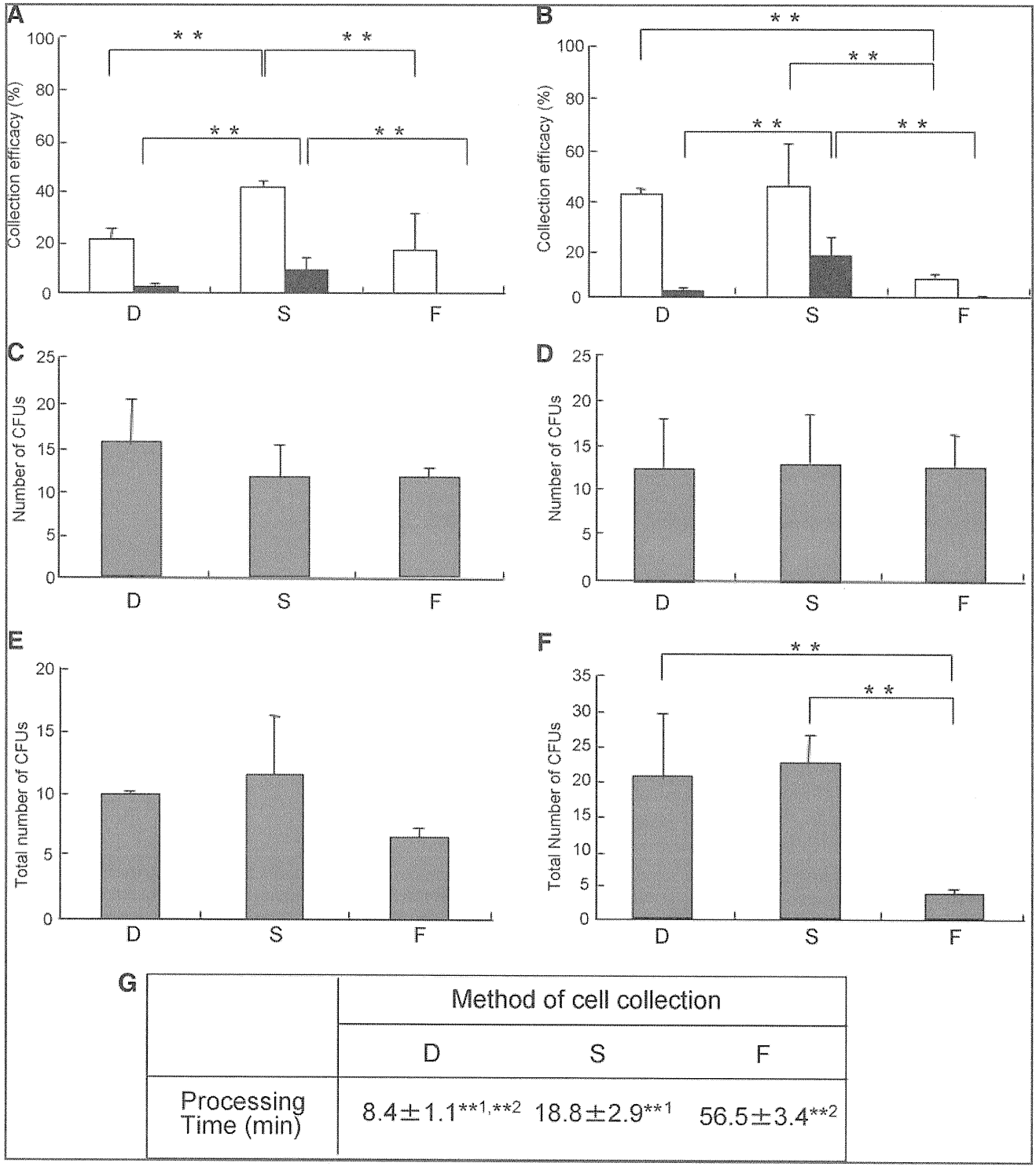

FIG. 3. Device selectively prepares MNCs with CFUs. Collection efficacy for MNCs (white box) and erythrocytes (black box) isolated with each method from canine (**A**) and human (**B**) bone marrow. D, S, or F indicates each method described in Materials and Methods section. $^{**}p < 0.01$. Number of CFUs derived from equal numbers (2.5×10^5) of MNCs isolated by each method from canine (**C**) and human (**D**) bone marrow. Total number of CFUs derived from equal amounts of canine (**E**) and human (**F**) bone marrow using each method. $^{**}p < 0.01$. (**G**) Processing time for each method. $^{**1}p < 0.01$; $^{**2}p < 0.01$.

Selective collection of colony-forming cells from bone marrow by the device

Next, the selectivity of the device was analyzed using cells derived from canine (Fig. 2E, F) and human (Fig. 2G, H) bone marrow. In both cases, most erythrocytes passed through the filter and were collected in the flow-through fraction. Only a few were found in the collected fraction (data not shown). For canine bone marrow, the number of MNCs was significantly smaller in the collected fraction than in the

flow-through fraction ($p = 0.002$; Fig. 2E). The number of CFUs, however, was much higher in the collected fraction ($p < 0.001$; Fig. 2F). For human bone marrow, the number of MNCs in the collected and flow-through fraction did not differ (Fig. 2G). However, the number of CFUs was much higher in the collected fraction than in the flow-through fraction ($p < 0.001$; Fig. 2H). These results indicated the selective collection of CFUs by the device.

Comparison of method D with methods S and F

The biological properties of cells isolated by each of the three methods were compared. First, we compared the collection efficacy of method D with that of method S or F. ANOVA revealed significant differences among the collection efficacies for MNCs (canine, $p = 0.024$; human, $p = 0.0002$). Comparisons between individual methods were then carried out using Turkey's *post hoc* test. For canine bone marrow, the collection efficacy for MNCs was significantly lower with method D ($20.7 \pm 4.2\%$) than method S ($41.6 \pm 1.6\%$) ($p < 0.01$; Fig. 3A), and the same between method D and method F ($16.8 \pm 14.0\%$) (Fig. 3A). As for contamination by erythrocytes, method S showed larger numbers than method D or F. For human bone marrow, there was no difference in collection efficacy between method D ($40.5 \pm 14.5\%$) and method S ($43.9 \pm 10.8\%$) (Fig. 3B), and method F ($7.3 \pm 1.8\%$) was significantly less efficient than method D ($p < 0.01$; Fig. 3B). The number of contaminating RBCs was again high with method S (Fig. 3B). Next, the MNCs collected by each method were seeded on plastic dishes, and the number of CFUs was counted 14 days later. ANOVA indicated no significant difference among the numbers of CFUs of MNCs prepared by the three methods in canine ($p = 0.40$) and human bone marrow ($p = 0.95$) (Fig. 3C, D). From the results on collection efficacy and number of CFUs, the total number of CFUs isolated from bone marrow was calculated for each method. In the case of canine bone marrow, the total number of CFUs with method D (10.1 ± 0.2) was equivalent to that with method S (11.7 ± 4.7) and much larger than that with method F, but not significant (6.6 ± 0.1) (Fig. 3E). Similar results were obtained with human bone marrow cells. The total number of CFUs with method D (20.3 ± 9.4) was equivalent to that with method S (22.3 ± 4.4), and much larger than that with method F (3.6 ± 1.0) ($p < 0.01$; Fig. 3F). These results indicated that the device collected colony-forming cells from bone marrow with an efficacy equal to that of current methods requiring centrifugation. In addition, the processing time for method D (8.4 ± 1.1 min; Fig. 3G) was significantly shorter than that for the other methods (method S, 18.8 ± 2.9 min; method F, 56.5 ± 3.4 min) (ANOVA, $p < 0.001$; Turkey's *post hoc* test, $p < 0.01$; Fig. 3G).

Expression of MSC markers in isolated BMSCs

To compare the cell population isolated by each of the three methods, the expression of cell surface markers was analyzed by fluorescence-activated cell sorting (FACS). Because a combination of markers is more reliable, we focused on $CD10^+/CD271^+$, $CD90^+/CD271^+$, or $CD106^+/STRO\text{-}1^+$ double-positive cells. The $CD90^+/CD271^+$ and the $CD106^+/STRO\text{-}1^+$ populations were significantly larger among cells collected by method D than those collected by method S or method F (ANOVA, $p < 0.001$; Turkey's *post hoc* test, $p < 0.01$ for $CD90^+/CD271^+$, $p < 0.05$ for $CD106^+/STRO\text{-}1^+$, respectively; Fig. 4A, B).

Differentiation potential of isolated BMSCs

To analyze their potential to differentiate, the BMSCs isolated by each of the methods were propagated on culture

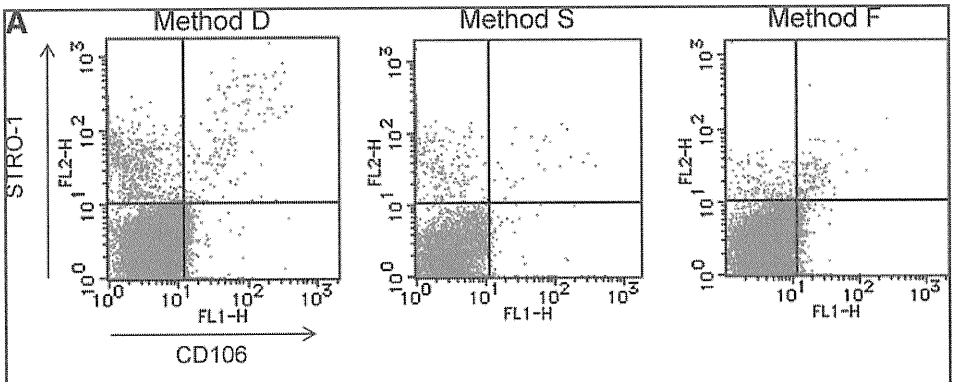

B

Markers	Fraction of double positive cells: Method D	Method S	Method F
$CD10^+$ / $CD271^+$	0.16 ± 0.05	0.13 ± 0.05	0.13 ± 0.02
$CD90^+$ / $CD271^+$	0.13 ± 0 **1**2	0.06 ± 0.01 **1*3	0.01 ± 0.01 **2*3
$CD90^+$ / $CD166^+$	0.31 ± 0.02	0.18 ± 0.12	0.23 ± 0.15
$CD106^+$ / $STRO\text{-}1^+$	1.61 ± 0.37 *1*2	0.48 ± 0.19 *1	0.71 ± 0.42 *2

FIG. 4. Device selectively prepares MNCs, which express mesenchymal marker. (**A**) FACS analysis of CD106 and STRO-1 on MNCs isolated by each method. (**B**) Fraction of cells double-positive for mesenchymal stem cell (MSC) markers among MNCs isolated by each method. **1,**2$p < 0.01$; *1,*2,*3$p < 0.05$.

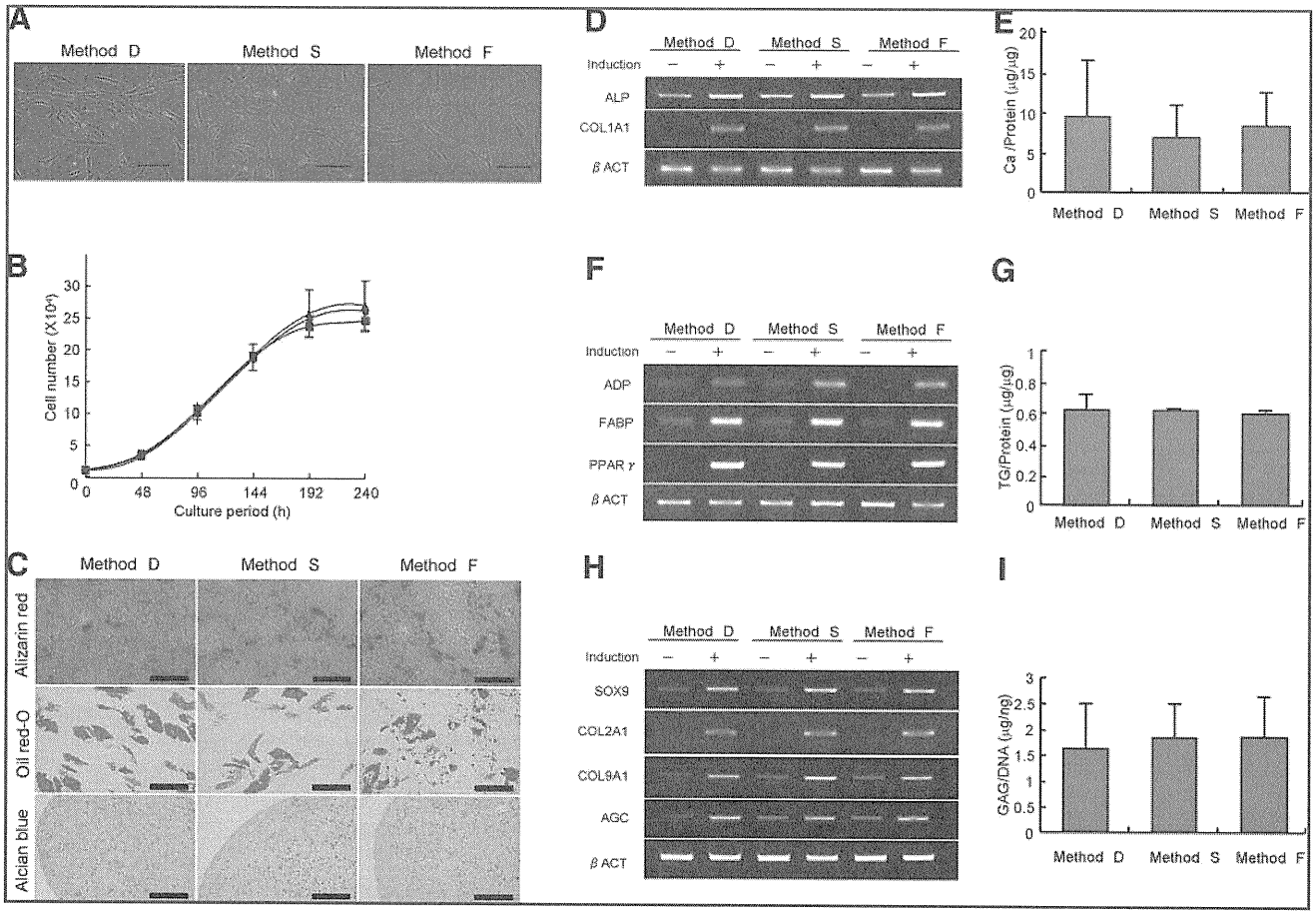

FIG. 5. Growth and differentiation potential of human BMSCs isolated by each method. The same numbers of BMSCs isolated by the three methods from human bone marrow were propagated on culture dishes for 2 weeks under standard conditions. (**A**) Microscopic views of cultured BMSCs isolated by each method. Magnification, 100×. Scale bars = 100 μm. (**B**) Growth of cultured BMSCs isolated by each method. ●, Method D; ▲, method S; ■, method F. (**C**) Differentiation potential of BMSCs isolated by each method. Osteogenic differentiation was analyzed by alizarin red staining. Magnification, 100×. Scale bars = 100 μm. Adipogenic differentiation was analyzed by oil red-O staining. Magnification, 100×. Scale bars = 100 μm. Chondrogenic differentiation was analyzed by alcian blue staining. Magnification, 40×. Scale bars = 300 μm. (**D**) Expression of bone-related genes before and after osteogenic induction. *ALP*, alkaline phosphatase. (**E**) Ca content after osteogenic induction. Ca, calcium. (**F**) Expression of fat-related genes before and after adipogenic induction. *ADP*, adipsin; *FABP*, fatty acid–binding protein; *PPARγ*, peroxisome proliferator-activated receptor gamma. (**G**) TG content after adipogenic induction. TG, triglyceride. (**H**) Expression of cartilage-related genes before and after chondrogenic induction. *AGC*, aggrecan. (**I**) GAG content after chondrogenic induction. GAG, glycosaminoglycan.

dishes and incubated for 2 weeks under standard growth conditions for MSCs. They were then induced to undergo osteogenesis, adipogenesis, and chondrogenesis. The morphology of the cells isolated by each of the methods was almost the same for both canine (Supplemental Fig. S2A, available online at www.liebertonline.com) and human (Fig. 5A) BMSCs. There was no difference in growth profile among the three methods in canine (Supplemental Fig. S2B, available online at www.liebertonline.com) or human (Fig. 5B) BMSCs. Osteogenic differentiation potential was evaluated with histochemical (alizarin red staining; Fig. 5C), mRNA expression (expression of the *ALP* and *COL1A1* genes; Fig. 5D), and biochemical (calcium content; Fig. 5E) analyses. There was no significant difference among the cells isolated by each of the three methods (ANOVA, $p = 0.61$). Similar results were observed in adipogenic differentiation

FIG. 6. Regeneration of bone tissues by cells isolated with the device. Data for six dogs at 4 weeks after the operation are presented. Frontal (**A**) and sagittal (**B**) views of micro-computed tomography. (**C**) Morphometrical analyses. The results of X-ray and micro-computed tomography were evaluated using the criteria described in the Materials and Methods section. Bone weight and volume were actually measured. $^{**}p < 0.01$; $^{*}p < 0.05$. CHR, carpal height ratio. (**D**) Histological analyses by hematoxylin–eosin staining. Magnification, 100×. Scale bar = 500 μm. (**E**) Fraction of regenerated bone tissue of each grade. Grade 1, white box; grade 2, gray box; grade 3, black box. $^{*}p < 0.05$. (**F**) Histological analyses using silver impregnation staining. Magnification, 200×. Scale bar = 200 μm. (**G**) Fraction of β-tricalcium phosphate with integrated collagen fibers of each grade. Grade 1, white box; grade 2, gray box; grade 3, black box. $^{*}p < 0.05$.

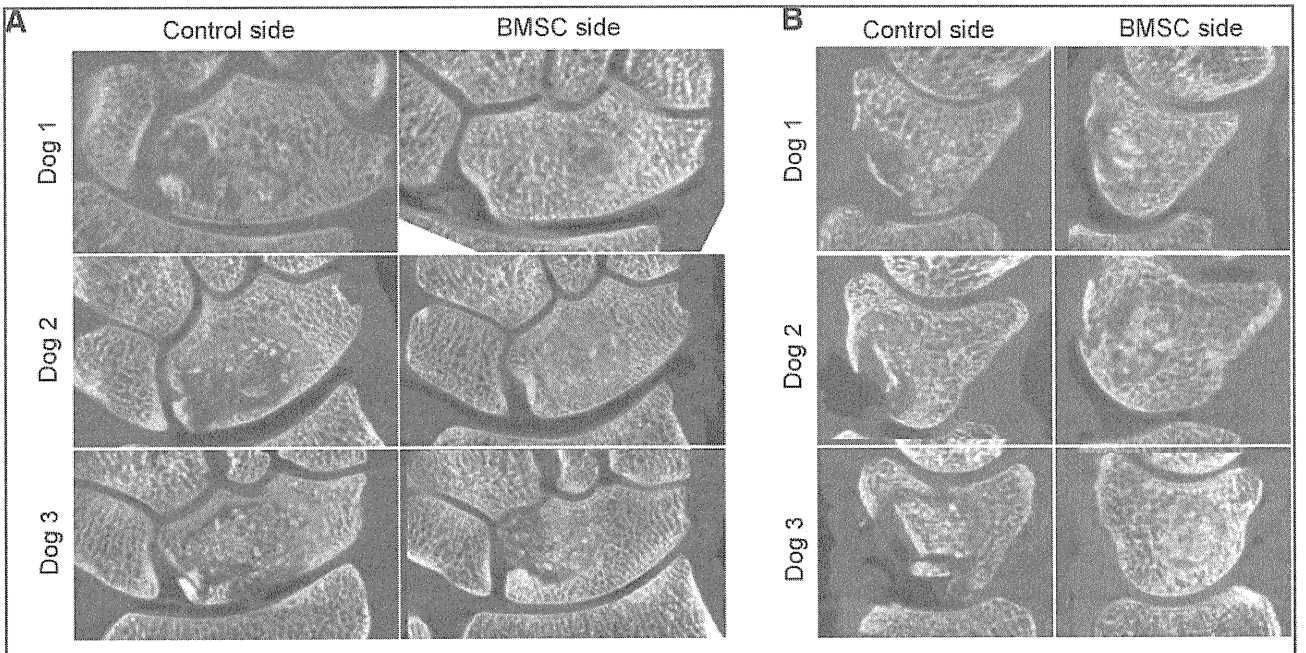

C

	X-ray evaluation		Micro CT evaluation			Actual Measurement		
	CHR	Ståhl index (%)	Bone Volume (cm^3)	Total Volume (cm^3)	Bone ratio	Weight (g)	Volume (cm^3)	Weight/Volume
Control side	0.30 ±0.03 * *	67.6 ±2.4 *	0.56 ±0.07 * *	0.81 ±0.11	0.67 ±0.03 * *	1.78 ±0.22 *	1.33 ±0.16 *	1.34 ±0.03 *
BMSC side	0.32 ±0.03 * *	72.1 ±6.3 *	0.64 ±0.06 * *	0.85 ±0.10	0.76 ±0.03 * *	1.83 ±0.19 *	1.34 ±0.15 *	1.38 ±0.04 *

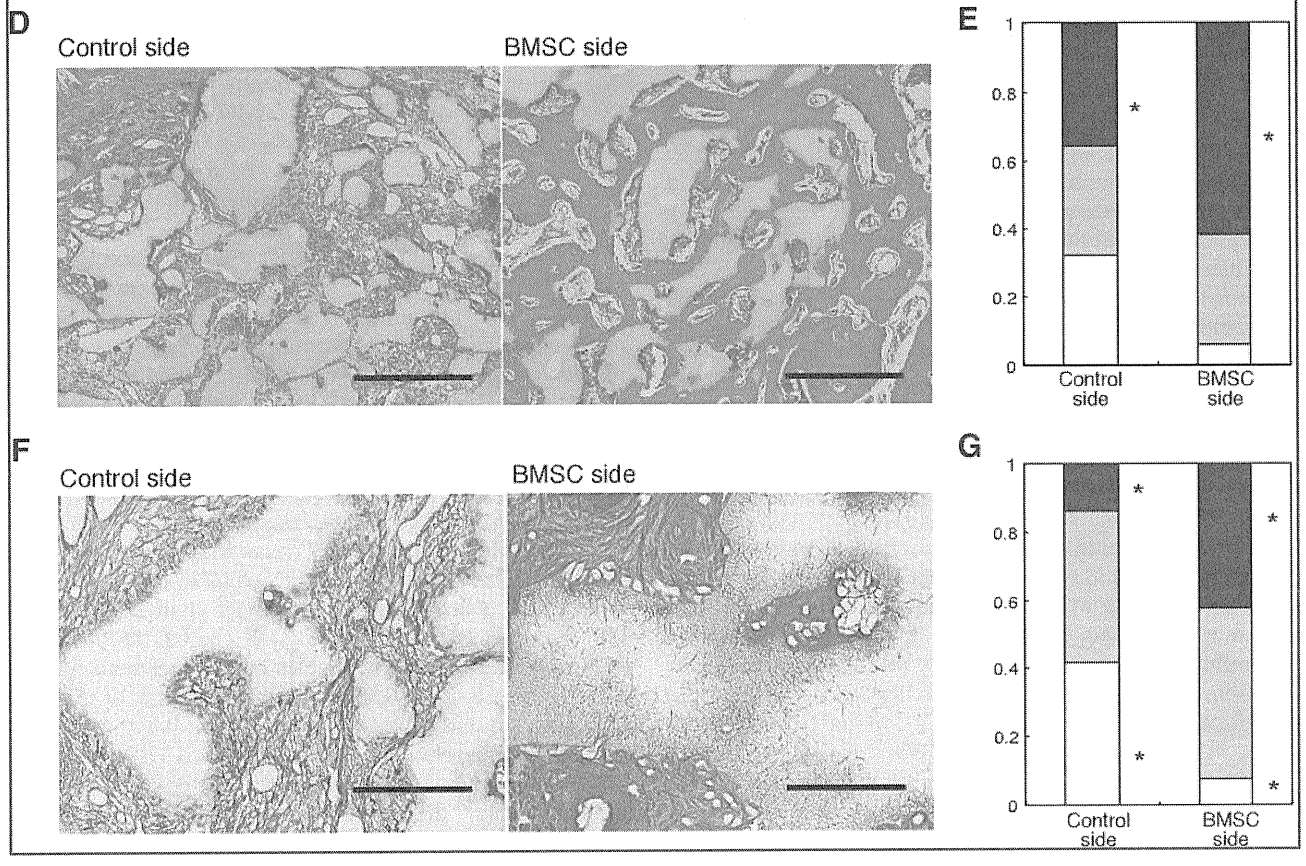

(ANOVA, $p = 0.41$; Fig. 5C, F, G) and chondrogenic differentiation (ANOVA, $p = 0.97$; Fig. 5C, H, I). Same results were obtained in the analyses of canine BMSCs (Supplemental Fig. S2C, available online at www.liebertonline.com). These results suggested that BMSCs isolated by each of the three methods had the multidirectional differentiation potential of MSCs.

Regeneration of bone tissues by cells isolated with the device

To confirm the *in vivo* osteogenic potential of cells collected with the device, we used the cells to regenerate bone tissues in a model of osteonecrosis using canine scapho-lunates, which we established previously.[15] Micro-CT findings at 4 weeks after the operation indicated bone regeneration to be more prominent on the BMSC side than control side in all cases (Fig. 6A, B). Carpal height ratio and the Ståhl index calculated from plain X-rays show the degree of collapse of scapholunate bone. Both parameters were significantly higher on the BMSC side than control side (Fig. 6C). Total volume and bone volume were analyzed from the micro-CT data. Bone volume and therefore bone ratio were greater on the BMSC side (Fig. 6C). Both actual weight and volume were also significantly higher on the BMSC side (Fig. 6C). These quantitative analyses suggested that the application of BMSCs prepared by the device contributed significantly to bone regeneration.

After the physical and radiological examinations, samples were processed for histological analyses. Microscopic findings of samples taken from the control side showed that a large amount of β-TCP remained unabsorbed, although multinucleated giant cells were found adjacent to β-TCP. In contrast, abundant new bone with the active absorption of β-TCP by multinucleated giant cells was found on the BMSC side (Fig. 6D). The extent to which β-TCP was absorbed as new bone formed was scored using criteria described in the Materials and Methods section. The grade 3 fraction was significantly larger on the BMSC side ($p = 0.032$; Fig. 6E).

To analyze the interaction between the prepared cells and β-TCP, silver impregnation staining was performed (Fig. 6F). The staining shows the invasion of collagen fibers into biodegradable materials. Collagen fibers in β-TCP granules adjacent to regenerated bone tissue were abundant on the BMSC side, but rare on the control side (Fig. 6F). Quantitative analyses showed the extent of the invasion to be significantly greater on the BMSC side ($p = 0.034$; Fig. 6G). These results suggested that BMSCs prepared using the device enhanced bone regeneration *in vivo*.

Discussion

Bone marrow cells consist of two types of MNCs: hematopoietic cells including hematopoietic stem cells, and stromal cells including MSCs. Approximately 99% of MNCs in bone marrow belong to the former population, and among the stromal cells, less than 5% have multidirectional differentiation potential compatible with the concept of MSCs. Therefore, the proportion of MSCs among bone marrow MNCs is estimated at less than 0.05%.[19] To obtain BMSCs including MSCs from bone marrow, it is essential to separate the hematopoietic MNCs.

Takenaka developed a novel filter composed of nonwoven fabrics to trap peripheral leukocytes for the treatment of autoimmune disease.[10] Because erythrocytes are deformed, which allows them to pass through small pores and have low adhesiveness, they can be separated from MNCs by the filter.[10] They used fibers 1.7 μm in diameter, because all the leukocytes were trapped when the fiber was less than 3 μm in diameter.[10] This filter, however, is not applicable to the separation of MSCs from hematopoietic MNCs, both of which will be captured, making it difficult to separate them by cell size. Therefore, we used fibers 15 μm in diameter with greater affinity for BMSCs than hematopoietic MNCs. MSCs are more adherent than hematopoietic cells.[4,19] MSCs adhere much more tightly to highly hydrophilic and rough surfaces than to hydrophobic and smooth surfaces.[20] The contact angle of the nonwoven fabric in the current device is estimated to be 20°, which is highly hydrophilic and may make it possible to trap MSCs in the device. This adherent trapping method may prevent excess shearing stress caused by the flow. Cells isolated by the device showed no increase in bradykinine or lactate dehydrogenase (LDH) (data not shown). In addition, mRNA expression of the *p16* and *p53* genes was not increased, and the karyotype showed no abnormalities (data not shown).

In terms of its potential clinical applications, the device has several advantages. The filter is composed of rayon and polyethylene. Rayon is used for the dialysis membranes of hemodialyzers and known to decrease platelet activity.[21] Polyethylene is a biomaterial employed in total hip replacement and as a scaffold for tissue engineering.[22] Therefore, all the materials are safe for clinical use. The isolation of BMSCs in a closed system is a major advantage of this device. Centrifugation requires mixing with an appropriate solution, which has to be performed in an open system. Current guidelines require the centrifugation process to be performed in an isolated area with specialized equipment. Because all steps can be done in a closed system, the device can isolate BMSCs from bone marrow on the operation table. Further, processing time is shorter than for the other two methods (Fig. 3G), which may help to reduce cell death during the isolation procedures. In addition, the method does not require special skills, which will help to obtain constant results and also be an advantage for clinical application.

We have shown that in terms of differentiation potential, the cells isolated using the device were equivalent to those prepared by current methods using centrifugation. The total number of CFUs obtained from bone marrow was equal to that achieved with method S and higher than that obtained with method F, suggesting that the device recovers almost all cells with the ability to form CFUs. FACS analyses showed that the method was superior to others in terms of the recovery of the MSC marker-positive population. CD10, CD44, CD90, CD106, and STRO-1 are considered surface markers of MSCs,[13,23] and, recently, CD271 was identified as a marker of MSCs.[24] The fractions of $CD90^+/CD271^+$ cells were larger among cells collected using the device than those isolated with the other two methods (Fig. 4). The $CD106^+/STRO\text{-}1^+$ fraction ($1.61 \pm 0.37\%$; Fig. 4) was even larger than that collected by FACS ($1.4 \pm 0.3\%$),[25] which has a risk of microbial contamination and unfavorable effects. We have no clear explanation for this selective collection. Because $CD106^+/STRO\text{-}1^+$ cells attach to plastic dish efficiently and have high colony-forming activity,[26] one possibility is that $CD106^+/STRO\text{-}1^+$ cells have high affinity to the filter materials used in the device. Finally, we have shown that the direct application of the trapped cells without *ex vivo* cultivation assisted the regeneration of bone

tissue *in vivo* (Fig. 6), although the role of transplanted cells may not be simply to reconstitute bone tissues by themselves but also to produce cytokines stimulating host cells,[15] suggesting that BMSCs collected with the new device on the operating table could be used for conditions requiring an acceleration of bone regeneration such as the nonunion of bone fractures.

Acknowledgments

We thank Dr. H. Iwata for suggestions and Drs. M. Neo, S. Fujibayashi, M. Takemoto, H. Ito, and H. Yoshitomi for clinical samples. This work was supported by Grants-in-aid for Scientific Research from the Japan Society for the Promotion of Science; from the Ministry of Education, Culture, Sports, Science, and Technology; from the Ministry of Health, Labor, and Welfare; and from the New Energy and Industrial Technology Development Organization.

Disclosure Statement

No competing financial interests exist.

References

1. Caplan, A.I. Mesenchymal stem cells. J Orthop Res **9,** 641, 1991.
2. Wagner, W., and Ho, A.D. Mesenchymal stem cell preparations comparing apples and oranges. Stem Cell Rev **3,** 239, 2007.
3. Peterson, E.A., and Evans, W.H. Separation of bone marrow cells by sedimentation at unit gravity. Nature **214,** 824, 1967.
4. Caterson, E.J., Nesti, L.J., Danielson, K.G., and Tuan, R.S. Human marrow-derived mesenchymal progenitor cells: isolation, culture expansion, and analysis of differentiation. Mol Biotechnol **20,** 245, 2002.
5. Li, Y., Ma, T., Yang, S.T., and Kniss, D.A. Thermal compression and characterization of three-dimensional nonwoven PET matrices as tissue engineering scaffolds. Biomaterials **22,** 609, 2001.
6. Takahashi, Y., and Tabata, Y. Effect of the fiber diameter and porosity of non-woven PET fabrics on the osteogenic differentiation of mesenchymal stem cells. J Biomater Sci Polym Ed **15,** 41, 2004.
7. Ma, Z., Kotaki, M., Yong, T., He, W., and Ramakrishna, S. Surface engineering of electrospun polyethylene terephthalate (PET) nanofibers towards development of a new material for blood vessel engineering. Biomaterials **26,** 2527, 2005.
8. Gador, W., and Jankowska, E. Filtration properties of nonwovens. Int J Occup Saf Ergon **5,** 361, 1999.
9. Gorman, N.E. Nonwoven materiel: manufacturing processes for sterilization wraps. Hosp Mater Manage Q **9,** 1, 1988.
10. Takenaka, Y. Lymphocytapheresis. Artif Organs **20,** 914, 1996.
11. Onodera, H., Abe, Y., Yoshida, M., Yamawaki, N., Yamashita, Y., Matsuo, H., Ichinose, K., Otsuru, I., and Shibuya, N. A new device for selective removal of $CD4^+$ T cells. Ther Apher **2,** 37, 1998.
12. Shibata, K.R., Aoyama, T., Shima, Y., Kenichi, F., Otsuka, S., Furu, M., Kohne, Y., Ito, K., Fujibayashi, S., Meo, M., Nakayama, T., Nakamura, T., and Toguchida, J. Expression of the p16INK4A gene is associated closely with senescence of human mesenchymal stem cells and is potentially silenced by DNA methylation during *in vitro* expansion. Stem Cells **25,** 2371, 2007.
13. Pittenger, M.F., Mackay, A.M., Beck, S.C., Jaiswal, R.K., Douglas, R., Mosca, J.D., Moorman, M.A., Simonetti, D.W., Craig, S., and Marshak, D.R. Multilineage potential of adult human mesenchymal stem cells. Science **284,** 143, 1999.
14. Fukiage, K., Aoyama, T., Shibata, K.R., Otsuka, S., Furu, M., Kohno, Y., Ito, K., Jin, Y., Fujita, S., Fujibayashi, S., Neo, M., Nakayama, T., Nakamura, T., and Toguchida, J. Expression of vascular cell adhesion molecule-1 indicates the differentiation potential of human bone marrow stromal cells. Biochem Biophys Res Commun **365,** 406, 2008.
15. Ikeguchi, R., Kakinoki, R., Aoyama, T., Shibata, K.R., Otsuka, S., Fukiage, K., Nishijo, K., Ishibe, T., Shima, Y., Otsuki, B., Azuma, T., Tsutsumi, S., Nakayama, T., Otsuka, T., Nakamura, T., and Toguchida, J. Regeneration of osteonecrosis of canine scapholunate using bone marrow stromal cells: possible therapeutic approach for Kienböck disease. Cell Transplant **15,** 411, 2006.
16. Youm, Y., McMurthy, R.Y., Flatt, A.E., and Gillespie, T.E. Kinematics of the wrist. I. An experimental study of radial-ulnar deviation and flexion-extension. J Bone Joint Surg Am **60,** 423, 1978.
17. Goldfarb, C.A., Hsu, J., Gelberman, R.H., and Boyer, M.I. The Lichtman classification for Kienböck's disease: an assessment of reliability. J Hand Surg Am **28,** 74, 2003.
18. Ogose, A., Kondo, N., Umezu, H., Hotta, T., Kawashima, H., Tokunaga, K., Ito, T., Kudo, N., Hoshino, M., Gu, W., and Endo, N. Histological assessment in grafts of highly purified beta-tricalcium phosphate (OSferion) in human bones. Biomaterials **27,** 1542, 2006.
19. Chamberiain, G., Fox, J., Ashton, B., and Middleton, J. Concise review: mesenchymal stem cells: their phenotype, differentiation capacity, immunological features, and potential for homing. Stem Cells **25,** 2739, 2007.
20. Kim, M.S., Shin, Y.N., Cho, M.H., Kim, S.H., Kim, S.K., Cho, Y.H., Khang, G., Lee, I.W., and Lee, H.B. Adhesion behavior of human bone marrow stromal cells on differentially wettable polymer surfaces. Tissue Eng **13,** 2095, 2007.
21. Thijs, A., Grooteman, M.P., Zweegman, S., Nubé, M.J., Huijgens, P.C., and Stehouwer, C.D. Platelet activation during haemodialysis: comparison of cuprammonium rayon and polysulfone membranes. Blood Purif **25,** 389, 2007.
22. Tessmar, J.K., and Göpferich, A.M. Customized PEG-derived copolymers for tissue-engineering applications. Macromol Biosci **7,** 23, 2007.
23. Deans, R.J., and Moseley, A.B. Mesenchymal stem cells: biology and potential clinical uses. Exp Hematol **28,** 875, 2000.
24. Bühring, H.J., Battula, V.L., Treml, S., Schewe, B., Kanz, L., and Vogel, W. Novel markers for the prospective isolation of human MSC. Ann NY Acad Sci **1106,** 262, 2007.
25. Gronthos, S., and Zannettino, A.C. A method to isolate and purify human bone marrow stromal stem cells. Methods Mol Biol **449,** 45, 2008.
26. Gronthos, S., Zannettino, A.C., Hay, S.J., Shi, S., Graves, S.E., Kortesidis, A., and Simmons, P.J. Molecular and cellular characterisation of highly purified stromal stem cells derived from human bone marrow. J Cell Sci **116,** 1827, 2003.

Address correspondence to:
Tomoki Aoyama, M.D., Ph.D.
Institute for Frontier Medical Sciences
Kyoto University
53 Kawahara-cho
Shogoin, Sakyo-ku
Kyoto 606-8507
Japan

E-mail: blue@frontier.kyoto-u.ac.jp

Received: December 21, 2008
Accepted: April 13, 2009
Online Publication Date: July 6, 2009

This article has been cited by:

1. Barbara Dozza, Claudia Di Bella, Enrico Lucarelli, Gianluca Giavaresi, Milena Fini, Pier Luigi Tazzari, Sandro Giannini, Davide Donati. 2011. Mesenchymal stem cells and platelet lysate in fibrin or collagen scaffold promote non-cemented hip prosthesis integration. *Journal of Orthopaedic Research* **29**:6, 961-968. [CrossRef]
2. Daisuke Kanematsu, Tomoko Shofuda, Atsuyo Yamamoto, Chiaki Ban, Takafumi Ueda, Mami Yamasaki, Yonehiro Kanemura. 2011. Isolation and cellular properties of mesenchymal cells derived from the decidua of human term placenta. *Differentiation* . [CrossRef]
3. Helena Motaln, Cristian Schichor, Tamara T. Lah. 2010. Human mesenchymal stem cells and their use in cell-based therapies. *Cancer* **116**:11, 2519-2530. [CrossRef]

Int. J. Dev. Biol. 55: 305-311 (2011)
doi: 10.1387/ijdb.103145tn

THE INTERNATIONAL JOURNAL OF DEVELOPMENTAL BIOLOGY
www.intjdevbiol.com

Highly efficient cryopreservation of human induced pluripotent stem cells using a dimethyl sulfoxide-free solution

TATSUYA NISHIGAKI[1], YUJI TERAMURA[2], AKIRA NASU[3], KEI TAKADA[4], JUNYA TOGUCHIDA[3] and HIROO IWATA*[,1]

[1]Department of Reparative Materials, Institute for Frontier Medical Sciences, [2]Radioisotope Research Center, [3]Department of Tissue Regeneration, Institute for Frontier Medical Sciences, [4]Laboratory of Cell Processing, Stem Cell Research Center, Institute for Frontier Medical Sciences, Kyoto University, Kyoto, Japan

ABSTRACT Human induced pluripotent stem (hiPS) cells have great potential for regenerative medicine and drug discovery. It is essential to establish highly efficient and reliable methods for hiPS cell cryopreservation. We examined cryopreservation of hiPS cells by the vitrification method using a dimethyl sulfoxide Me_2SO-free and serum-free medium, VS2E, that uses Euro-Collins solution as a base with 40% (v/v) ethylene glycol and 10% (w/v) polyethylene glycol as cryoprotectants. This combination of vitrification and cryoprotectants resulted in a higher recovery rate of hiPS cells than with a commercially-available vitrification solution, DAP213, which contained Me_2SO and serum components. After vitrification and warming, hiPS cells were cultured easily. Even after several subculturing steps, cells expressed undifferentiated cell markers, such as Oct-3/4 and SSEA-4, and also exhibited alkaline phosphatase activity. The pluripotency of hiPS cells was maintained, as demonstrated by teratoma formation upon hiPS cell transplantation into severe combined immunodeficient mice. Thus, we successfully preserved hiPS cells under liquid nitrogen with high efficiency using Me_2SO-free vitrification solution and rapid cooling.

KEY WORDS: *cryopreservation, human induced pluripotent stem (iPS) cell, vitrification, Me_2SO-free, ethylene glycol*

Introduction

Human embryonic stem (hES) and induced pluripotent stem (hiPS) cells are important in regenerative medicine and in drug discovery due to their pluripotent potential (Keller and Snodgrass, 1999; Ameen *et al.*, 2008; Nakagawa *et al.*, 2008; Takahashi *et al.*, 2007; Yu *et al.*, 2007). It is essential to establish methods for stably storing these stem cells, especially hiPS cells derived from patients with obstinate diseases. Cryopreservation using conventional slow-freezing methods results in low hiPS cell survival after thawing; further, a long culture period (at least 2 weeks) is required after thawing before experiments can be conducted (Reubinoff *et al.*, 2001; Fujioka *et al.*, 2004). Efficient cryopreservation and subsequent culture thus remain an obstacle to the effective use of hiPS.

Cryopreservation protocols developed for hES cells (Reubinoff *et al.*, 2001; Fujioka *et al.*, 2004; Richards *et al.*, 2004; Ji *et al.*, 2004) have also been used for hiPS cell cryopreservation. Although cell survival is improved compared to conventional methods, there is still room for improvement. Most cryopreservation media contain fetal bovine serum or serum-replacement and dimethyl sulfoxide (Me_2SO). Ideally, components from animal serum or serum-replacement should not be included in the culture media to reduce the risks of infection by unknown pathogens in future regenerative medicine applications. Me_2SO [~1% (v/v)] has been used for ES cell differentiation into mesendoderm (Ameen *et al.*, 2008), and cryopreservation with slow freezing method using Me_2SO reportedly induces ES cell differentiation (Katkov *et al.*, 2006). Therefore, it is desirable to develop a cryopreservation medium that lacks both Me_2SO and animal-derived components. Recently, the cryopreservation recovery ratios of hES and hiPS cells was improved by using Rho-associated coiled-coil kinase (ROCK) inhibitor (Martin-Ibañez *et al.*, 2008; Li *et al.*, 2009; Claassen *et al.*, 2009; Mollamohammadi *et al.*, 2009); however, cryopreservation with the ROCK inhibitor is

Abbreviations used in this paper: DSC, differential scanning calorimeter; hES, human embryonic stem cell; hiPS, human induced pluripotent stem cell; SPR, surface plasmon resonance; SUV, small unilamellar vesicle; tBLM, tethered bilayer membrane.

***Address correspondence to:** Hiroo Iwata. Department of Reparative Materials, Institute for Frontier Medical Sciences, Kyoto University, 53 Kawara-Cho, Shogoin, Sakyo-ku, Kyoto, 606-8507, Japan. Fax: +81-75-751-4119. e-mail: iwata@frontier.kyoto-u.ac.jp

Supplementary Material (two figures) for this paper is available at: http://dx.doi.org/10.17

Accepted: 18 August 2010. *Final, author-corrected PDF published online:* 15 June 2011.

ISSN: Online 1696-3547, Print 0214-6282

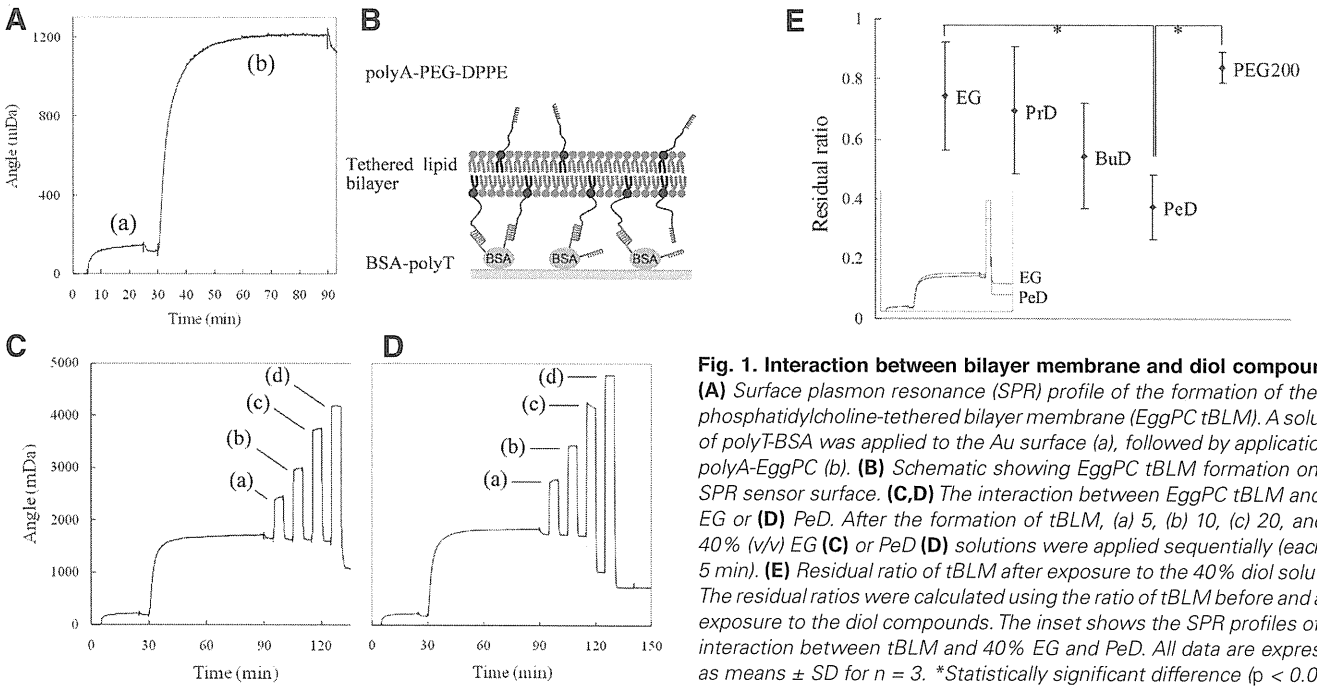

Fig. 1. Interaction between bilayer membrane and diol compounds. **(A)** *Surface plasmon resonance (SPR) profile of the formation of the L-α-phosphatidylcholine-tethered bilayer membrane (EggPC tBLM). A solution of polyT-BSA was applied to the Au surface (a), followed by application of polyA-EggPC (b).* **(B)** *Schematic showing EggPC tBLM formation on the SPR sensor surface.* **(C,D)** *The interaction between EggPC tBLM and* **(C)** *EG or* **(D)** *PeD. After the formation of tBLM, (a) 5, (b) 10, (c) 20, and (d) 40% (v/v) EG* **(C)** *or PeD* **(D)** *solutions were applied sequentially (each for 5 min).* **(E)** *Residual ratio of tBLM after exposure to the 40% diol solution. The residual ratios were calculated using the ratio of tBLM before and after exposure to the diol compounds. The inset shows the SPR profiles of the interaction between tBLM and 40% EG and PeD. All data are expressed as means ± SD for n = 3. *Statistically significant difference (p < 0.05).*

very time consuming, and the inhibitor might affect cell function. Thus, a simpler and more reliable method is needed.

Our group recently developed vitrification solutions for the cryopreservation of pancreatic islets and primate ES cells (Agudelo and Iwata, 2008; Agudelo *et al.*, 2009; Nishigaki *et al.*, 2010). These solutions do not contain Me_2SO and animal-derived components; rather, the main components are ethylene glycol (EG) and Euro-Collins solution. Our results suggested that diol compounds could replace Me_2SO for cryopreservation. In the present study, we systematically examined the use of diol compounds, including EG, propane diol (PrD), butane diol (BuD), pentane diol (PeD), and polyethylene glycol (MW 200; PEG200) to improve the survival rate of hiPS cells after cryopreservation by vitrification. An alkaline phosphatase activity assay and immunostaining for Oct4 and SSEA-4 were performed to evaluate the differentiation status of the hiPS cells. The potency of hiPS cells to differentiate into three germ lines was also examined by transplantation of hiPS cells into severe combined immunodeficient (SCID) mice after the vitrification and warming procedure.

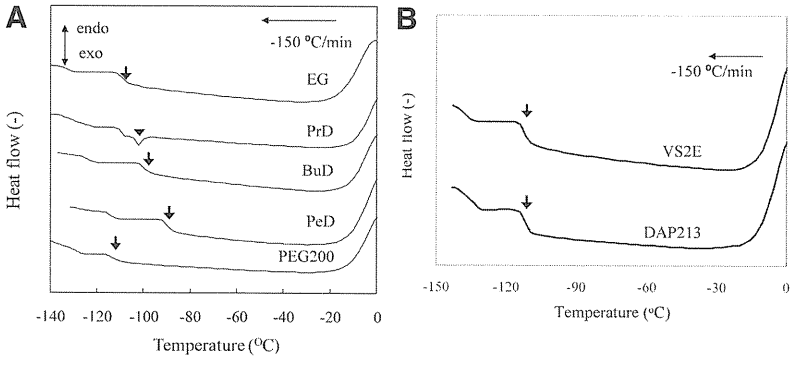

Fig. 2. Thermal analysis of (A) 40% diol compound solutions in Euro-Collins solution and (B) VS2E and DAP213 solution using differential scanning calorimetry (DSC). *The chamber was cooled from 0 to -140°C at a rate of -150°C/min. Arrows indicate changes in the slope, and an arrowhead indicates an exothermic peak.*

Results and Discussion

Effects of diol solutions on tBLM

In this study, we examined the use of four diol compounds, HO-$(CH_2)_n$-OH (n = 2-5), and poly(ethylene glycol) HO-$(CH_2CH_2O)_n$-H as cryoprotectants in a vitrification solution for hiPS cells. Surface plasmon resonance (SPR) was employed to investigate the interaction between a cell membrane and the diol compounds *in vitro*. A tethered bilayer membrane (tBLM) was formed on the SPR sensor surface and exposed to solutions with different concentrations of diols. tBLMs were prepared using the vesicle fusion method on a hydrophilic surface (Taylor *et al.*, 2007; Chung *et al.*, 2009). First, polyT-BSA was adsorbed on the SPR sensor surface, and then a suspension of polyA-PEG-DPPE-modified SUVs was applied to the surface. PolyT-BSA was effectively adsorbed on the Au surface (Fig. 1Aa). The largest shift increase (~1 DA) was observed in the SPR profile when polyA-EggPC was applied to the polyT-BSA-modified sensor surface (Fig. 1Ab), indicating the formation of tBLM as shown schematically in Fig. 1B.

A cell membrane consists of a thin lipid bilayer that contains membrane proteins. The effects of diol compounds on cell membranes were examined by SPR using tBLM as a cell membrane model. The EggPC tBLM was exposed to increasingly concentrated diol solutions containing 5, 10, 20, and 40% (v/v) of diol in PBS for 5 min each, and then the surfaces were washed with PBS for 5 min. The SPR signal intensities were monitored to determine whether diol compounds damaged the tBLM. Fig. 1 C,D show the SPR profiles

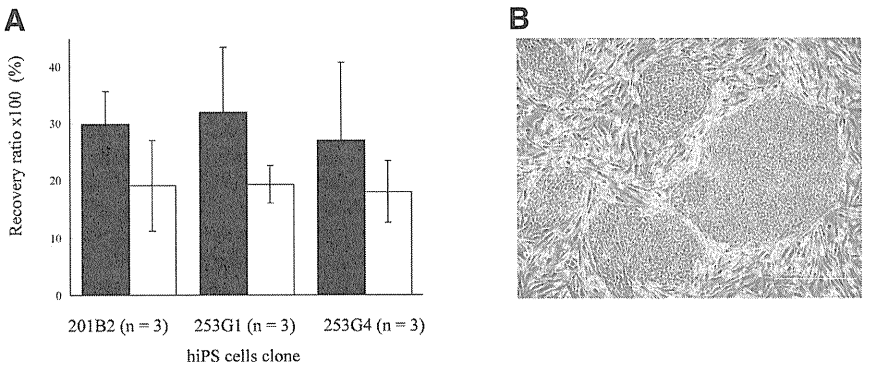

Fig. 3. Recovery rates of hiPS cells and colonies formed by hiPS cells after freezing and thawing. (A) *Recovery rates of hiPS cells (clones: 201B2, 253G1, 253G4) 1 day after the cryopreservation and thawing procedure. hiPS cell were cryopreserved in VS2E (black bars) or DAP213 (white bars). The recovery rates were calculated by comparing the number of colonies 1 day after thawing/culture to the number of colonies formed by cells that were not cryopreserved. Results are expressed as means ± SD for n = 3.* **(B)** *A phase contrast microscope image of cultured 253G1 hiPS cells that were cryopreserved in VS2E 3 days after thawing. Scale bar: 500 μm.*

when tBLMs were exposed to diol solutions of 5, 10, 20, and 40% (v/v) EG or PeD, respectively. There was no change in the SPR signal intensity when the tBLM was washed with PBS after a 5, 10, or 20% EG solution was applied, but the SPR signal intensity decreased after the 40% EG was applied. These results suggested that the tBLM remained intact when exposed to up to 20% EG but was damaged upon exposure to 40% EG. For PeD, the decrease in the SPR signal intensity began upon exposure to 20% PeD; thus, PeD interacted with or damaged the lipid bilayer membrane at lower concentrations than did EG. These experimental results indicated that the greater the hydrophobicity of the diol solution, the greater the damage to the cell membrane.

Fig. 1E shows the relative amounts of the residual lipid bilayer membrane when tBLM was exposed to 40% diol solutions. The amount of residual membrane decreased with increased diol molecular weight. The exception was PEG200: although it was the highest molecular weight compound used in this study, it did not damage the tBLM very much. PEG is a hydrophilic molecule, so presumably there was little or no interaction with the lipid bilayer membrane. In general, hydrophobic diol compounds with longer alkyl chain damaged the bilayer membrane.

Thermal properties of cryopreservation solutions during the cooling process

Effective vitrification is important for cryopreservation of hiPS cells. DSC analyses were carried out to monitor ice crystal formation in solutions of diol compounds in Euro-Collins solution. Fig. 2A shows DSC charts of 40% (v/v) diol solutions during cooling at a rate of -150°C/min. The slopes of the DSC curves of EG, BuD, PeD, and PEG200 solutions changed at around -110, -100, -90, and -115°C (indicated by arrows). Those points indicate when the glass-transition phase change occurred. When the solutions in cryotubes were immersed directly into liquid nitrogen, the solutions remained transparent. These data indicate that the diol solutions were vitrified effectively. However, an exothermic peak was observed for the PrD solution at around -105°C, as indicated by an arrowhead in Fig. 2A. This could be attributed to crystallization of the PrD solution, and indeed it has been reported that PrD tends to form intermolecular hydrogen bonds in water (Takamuku *et al.*, 2008), indicating long-range ordering. This might lead to crystallization.

The thermal analyses suggested that EG, BuD, PeD, and PEG200 were suitable for use in a vitrification solution. The SPR studies (Fig. 1) indicated that diols with shorter alkyl chain were less harmful to the artificial cell membrane.

Vitrification of hiPS cells

A vitrification solution of human ES cells (VS2E) was prepared using EG, PEG200, and Euro-Collins solution (Nishigaki *et al.*, 2010). We examined various diols and their different concentrations to find a more suitable diol than EG for vitrification of hiPS cells (*see Supplemental information*). Although we had expected to find a more suitable diol than EG for vitrification, the results shown in *Supplemental Fig. 1 and 2* indicated that EG was the most suitable diol for use in a vitrification solution. In this study, we examined VS2E solution to cryopreserve hiPS cells, because various characters of hiPS cells are similar to those of hES cells.

A commercially available solution that contains Me_2SO and serum components, DAP213, is currently used for cryopreservation of ES cells and iPS cells. We compared vitrification using our solution, VS2E, with vitrification using DAP213. The compositions of these solutions are shown in Table 1. These cryopreservation solutions were analyzed using DSC (Fig. 2B) at a cooling rate of -150°C/min. No exothermic peak was observed for crystallization in either the DAP213 or VS2E solution. The slope changes around -110°C, indicating the glass-transition phase change (arrows in Fig. 2B), were observed for both solutions. Both solutions remained transparent after immersion into liquid nitrogen. These results indicate the two solutions were vitrified by rapid cooling.

hiPS cells (253G1, 253G4, and 201B2) were preserved in liquid nitrogen using a combination of rapid cooling and vitrification solution VS2E or DAP213. The recovery rates of these hiPS after vitrification and warming are summarized in Fig. 3A, and a phase contrast microscope image of hiPS cells cultured for 3 days is shown in Fig. 3B. The recovery rates of hiPS cell clones 201B2, 253G1, and 253G4, preserved by vitrification using VS2E were 29.8 ± 5.8% (n = 3), 32.0 ± 11.4% (n = 3), and 27.1 ± 13.6% (n = 3), respectively. There was no significant difference in the

TABLE 1

COMPOSITION OF THE CRYOPRESERVATION SOLUTIONS

	VS2E	DAP213
Me_2SO % (v/v)	–	14.2
EG % (v/v)	40	–
PG % (v/v)	–	22
PEG % (w/v)	10	–
Acetamide % (w/v)	–	5.9
DMEM/F12 with KSR	–	+
Euro-Collins	+	–

Me_2SO: dimethyl sulfoxide; EG: ethylene glycol; PG: propylene glycol; PEG: polyethylene glycol (MW1000); DMEM/F12: Dulbecco's modified Eagle medium/F12; KSR: knockout serum replacement; Euro-Collins: 34.95 g/L dextrose, 7.3 g/L K_2HPO_4, 2.04 g/L KH_2PO_4, 1.12 g/L KCl, and 0.84 g/L $NaHCO_3$.

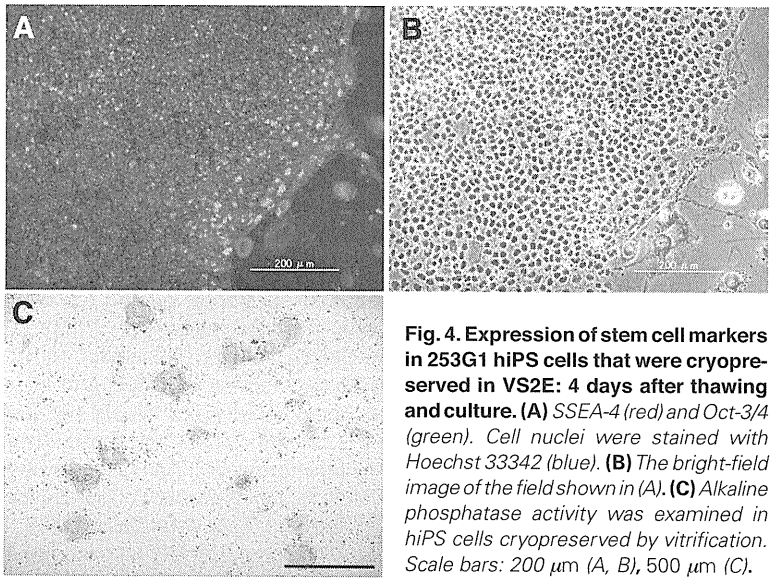

Fig. 4. Expression of stem cell markers in 253G1 hiPS cells that were cryopreserved in VS2E: 4 days after thawing and culture. (A) *SSEA-4 (red) and Oct-3/4 (green). Cell nuclei were stained with Hoechst 33342 (blue).* **(B)** *The bright-field image of the field shown in (A).* **(C)** *Alkaline phosphatase activity was examined in hiPS cells cryopreserved by vitrification. Scale bars: 200 μm (A, B),* 500 *μm (C).*

recovery rates of the different clones. In addition, all of the hiPS cells proliferated well and those could be subcultured 3 days after seeded. These results indicated that the VS2E solution developed for vitrification of hES cells was suitable for cryopreservation of hiPS cells as well. In contrast, the recovery rates of hiPS cell clones 201B2, 253G1, and 253G4, preserved by vitrification using the commercially available solution, DAP213, were 19.3 ± 3.3% (n = 3), 18.0 ± 5.4% (n = 3), and 19.1 ± 8.0% (n = 3), respectively.

Although the differences in recovery rates using VS2E and DAP213 were not significant, the recovery rates for the VS2E solution tended to be higher than those for DAP213. Although DAP213 is an effective vitrification solution (Fig. 3A), VS2E is preferable because it is free of Me_2SO and serum components. In a series of experiments, we also cryopreserved hiPS cells (clone 253G1) using a conventional slow freezing method with 10% Me_2SO. Only a few colonies were formed after cryopreservation and thawing (data not shown) and it took 3 to 4 weeks to subculture hiPS cells. These results indicated that the slow freezing method is not suitable for cryopreservation of hiPS cells.

After hiPS cells were cryopreserved with VS2E and subsequently cultured for 4 days, colonies were analyzed immunohistochemically for undifferentiated cell markers SSEA-4 and Oct3/4 (Thomson *et al.*, 1998; Sperger *et al.*, 2003). The alkaline phosphatase activity of the hiPS cells was visualized after fixation with PFA. The hiPS cells exhibited alkaline phosphatase activity and expressed SSEA-4 and Oct3/4 (Fig. 4). The undifferentiated state was thus maintained in the hiPS cells after cryopreservation in VS2E under liquid nitrogen, thawing, and culture.

The pluripotency of the hiPS cells was examined by transplantation into SCID mice. Twelve weeks after transplantation, the teratomas formed from the injected cells were removed for histological examination. Fig. 5 shows HE-stained tissue sections from the teratomas. Endodermal epithelium, mesoderm-derived cells (muscle, cartilage), and neuroepithelium were identified in teratomas formed from 253G1 hiPS cells. Thus, histological analyses of the teratomas revealed that cryopreserved hiPS cells vitrified using VS2E and preserved under liquid nitrogen retained their pluripotency.

We meet some difficulties in cryopreservation of cells by vitrification. Those are troublesome procedures, a tube container with small diameter, the use of Me_2SO, and contamination risk from the direct contact with liquid nitrogen. In this study, we made some improvement in cell vitrification, such as use of a conventional cryotube, the simple solution without Me_2SO, and simple procedure.

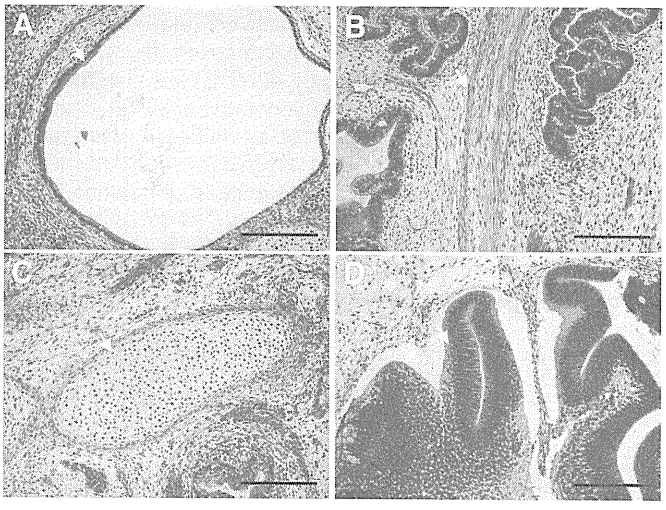

Fig. 5. Teratoma formation in SCID mice after transplantation of 253G1 hiPS cells cryopreserved in VS2E solution. *Arrows indicate* **(A)** *endodermal epithelium,* **(B)** *muscle,* **(C)** *cartilage, and* **(D)** *neuroepithelium. Scale bars: 200 μm.*

Conclusion

We successfully cryopreserved and recovered hiPS cells using a vitrification solution composed of 40% (v/v) EG and 10% (v/v) PEG in Euro-Collins solution. EG was the most suitable diol compound for use in the vitrification solution. hiPS cells could be preserved under liquid nitrogen using VS2E solution combined with rapid cooling. The recovery rates were around 30%, and the hiPS cells maintained pluripotency after cryopreservation using liquid nitrogen and subsequent thawing and culture. The cryopreservation solution VS2E thus has great potential for use in experimental research as well as in medical applications of hiPS cells.

Experimental Protocols

Surface plasmon resonance (SPR)

In this paper, we examined the interaction between diol compounds and a tethered bilayer membrane (tBLM) *in vitro* using an SPR apparatus to elucidate the influence of diol compounds on a living cell membrane (Pavey *et al.*, 1999; Green *et al.*, 1997). The tBLM was fabricated by the vesicle fusion method using small unilamellar vesicles (SUVs) on a hydrophilic surface (Taylor *et al.*, 2007; Chung *et al.*, 2009).

Synthesis of polyA-PEG-DPPE and polyT-BSA

α-*N*-Hydroxysuccinimidyl-ω-maleimidyl poly(ethylene glycol) (NHS-PEG-Mal, Mw: 5000) and 1,2-distearyl-*sn*-glycerol-3-phosphatidylethanolamine (DSPE) were purchased from the NOF Corporation (Tokyo, Japan). Mal-PEG-DPPE was synthesized by first dissolving NHS-PEG-Mal (180 mg), triethylamine (50 μL, Nacalai Tesuque, Kyoto, Japan), and DPPE

(20 mg) in dichloromethane (Nacalai Tesuque) and stirring for 36 h at RT (Teramura *et al.*, 2010a; Teramura *et al.*, 2010b; Teramura *et al.*, 2007). A white powder (190 mg, yield 80%) was obtained by precipitation of the reaction mixture with diethyl ether. ^{1}H-NMR ($CDCl_3$, 400 MHz, δ ppm): 0.88 (t, 6H, -CH_3), 1.25 (br, 56H, -CH_2-) 3.64 (br, 480H, PEG), 6.71 (s, 2H, -HC=CH-, maleimide).

Poly(adenosine phosphate) (20) (polyA) and poly(thymidine phosphate) (20) (polyT) carrying protected SH group at the 5'-ends were purchased from Sigma-Aldrich Chemical Co. (St. Louis, MO, USA). PolyA with a 5'-end SH group was prepared by reduction of the disulfide bond with DTT according to the manufacturer's instructions. The SH groups were conjugated to the Mal-PEG-lipid to prepare polyA-PEG-lipid. PolyA-SH (1.0 mg) was mixed with Mal-PEG-DPPE (5.0 mg) in PBS and incubated for 24 h at RT to prepare polyA-PEG-lipid (500 μg/mL in PBS). PolyT-PEG-DPPE was prepared the same way as polyA-PEG-DPPE.

Bovine serum albumin (BSA) (Cohn V fraction, Sigma) in PBS (500 μL of a 20 mg/mL solution) was mixed with 20 μL of 62.2 mg/mL sulfo-EMCS (*N*-(6-maleimidocaproyloxy) sulfo-succinimide, sodium salt; Thermo Scientific, USA) and incubated for 2 h at RT to introduce maleimide groups onto the BSA. Maleimide-conjugated BSA (BSA-Mal) was purified with a Sephadex™ G-25 M column (GE Healthcare UK Ltd., Buckinghamshire, UK). BSA-Mal solution (8.2 μL of a 10 mg/mL solution) was mixed with 90 μL of a 1.78 mg/mL polyT-SH solution, and the reaction mixture was incubated for 2 h at RT. This reaction mixture was used as a polyT-BSA solution.

Small unilamellar vesicles (SUVs)

L-α-phosphatidylcholine (EggPC, Sigma) was dissolved in chloroform and put in a flask. The chloroform was removed to prepare a dry thin lipid film using a rotary evaporator. PBS was added to the lipid film and stirred vigorously at 4°C for 4 days to prepare lipid vesicles (lipid concentration = 10 mg/mL). The suspension was then extruded through membrane filters with pore size 0.8 μm, 0.22 μm (2 times), and 0.1 μm (10 times) to form SUVs (~100 nm diameter). PolyA-EggPC was prepared by incubation of SUVs with polyA-PEG-DPPE for 1 h at 37°C.

SPR measurements

Glass plates (BK7, refractive index: 1.515, size: 25 × 25 × 1 mm, Arteglass Associates Co., Kyoto, Japan) were immersed for 5 min in a piranha solution (a 7:3 mixture of concentrated sulfuric acid and 30% hydrogen peroxide), washed three times with deionized water, rinsed three times with Milli-Q water and three times with 2-propanol, and finally stored in 2-propanol until use. The glass plates were dried under a stream of nitrogen gas and then mounted on the rotating stage of a thermal evaporation coating apparatus (V-KS200, Osaka Vacuum, Ltd., Osaka, Japan). A 1-nm chromium layer was deposited, and then a 49-nm gold layer was deposited.

This study used an SPR apparatus that was constructed in our laboratory (Hirata *et al.*, 2000). A flow chamber with a gold-covered glass plate was placed on the prism of the SPR apparatus, and PBS was circulated at a flow rate of 4.0 mL/min in the flow chamber for at least 5 min. The reflectivity of a *p*-polarized HeNe laser beam (λ = 632.8 nm) from the sample unit was monitored as a function of the incident angle. The least-squares method of the quadratic function was applied to points around the point of maximum loss of reflectivity, and the minimum point described by this fitted curve was defined as the resonance angle. The incident angle was then fixed at 0.5° less than the resonance angle. For construction of a tethered bilayer membrane (tBLM), a 30 μg/mL polyT-BSA solution in PBS was introduced into the flow chamber, allowed to adsorb onto the Au surface for 20 min, and then a 100 μg/mL polyA-EggPC solution in PBS was circulated for 1 h. To determine whether the diol solutions damaged the membrane, the EggPC tBLM was exposed to diol solutions [5, 10, 20, and 40% (v/v) EG or PeD in PBS] for 5 min, then washed with PBS for 5 min. To express the degree of damage to the EggPC tBLM, the residual ratio of the EggPC tBLM was calculated as follows:

Residual ratio = (SPR angle shift after exposure to the diol solution) / (SPR angle shift of the EggPC tBLM from the sensor surface).

DSC measurements

A differential scanning calorimeter (DSC, Diamond DCS, PerkinElmer, Inc. MA, USA) was used for thermal analysis of the cryopreservation solutions during the cooling process. The sample solutions were cooled from 0°C to -140°C at a rate of -150°C/min.

hiPS cell culture

hiPS cell line 253G4, established by transfection with OCT3/4, SOX2, and KLF4 (Nakagawa *et al.*, 2008), and cell line 201B2, established by transfection with OCT3/4, SOX2, KLF4, and MYC, were the kind gift of Prof. Shinya Yamanaka. The hiPS cell line 253G1, established by transfection with OCT3/4, SOX2, and KLF4, was obtained from the RIKEN cell bank, Japan. Undifferentiated hiPS cells were maintained on a feeder layer of SNL76/7 cells (Thomas *et al.*, 1987) treated with mitomycin C (Wako Pure Chemical, Osaka, Japan). SNL76/7 cells are a mouse fibroblast STO cell line that expresses the neomycin-resistance gene cassette and LIF (ECACC, UK). The undifferentiated hiPS cells and SNL76/7 feeder cells were cultured in Dulbecco's modified Eagle medium/F12 (DMEM/F12, Sigma) supplemented with 20% (v/v) knockout serum replacement (KSR; Invitrogen, Carlsbad, CA), 0.1 mM nonessential amino acid (NEAA, Invitrogen), 2 mM L-glutamine (Sigma), 0.1 mM 2-mercaptoethanol (Sigma), 5 mM sodium hydroxide, and 5 ng/mL FGF2 (Kaken Pharmaceutical Co., Ltd., Tokyo, Japan) in a humidified atmosphere of 5% CO_2 and 95% air at 37°C. The hiPS cells were subcultured every 4–5 days using 0.25% (v/v) trypsin and 0.1 mg/mL collagenase (Type S-1, Nitta Gelatin Inc., Osaka, Japan) in PBS (-) supplemented with 20% (v/v) KSR and 1 mM calcium chloride. The hiPS cells were suspended in PBS as cell clumps, but not single cells. SNL76/7 cells were routinely maintained in DMEM (Sigma) supplemented with 10% (v/v) fetal bovine serum (FBS, Equitech-Bio, Inc. TX, USA).

Vitrification of hiPS cells

Liquid nitrogen preservation

We examined the cryopreservation of hiPS cells using VS2E vitrification solution as well as the DAP213 vitrification solution developed by Fujioka *et al.*, 2004. The compositions of the solutions are listed in Table 1. The VS2E and DAP213 solutions were sterilized by filtration through a membrane (φ: 0.22 μm) before use. Confluent hiPS cells in 60 mm dishes were harvested by treatment with trypsin and collagenase as described above. A pellet of hiPS cells was collected by centrifugation at 1000 rpm for 5 min and resuspended in 200 μL of a vitrification solution in a cryotube (1.8 mL, CryoTube™ Vials, Nunc™, Denmark). The cryotube was immediately immersed in liquid nitrogen and stored for 7 days until recovery rate determination was conducted.

Recovery rate of hiPS cells after liquid nitrogen preservation

Culture medium (1 mL) pre-warmed to 37°C was added directly to vitrified hiPS cells (200 μL) in the cryotube, followed by rapid pipetting. The hiPS cell suspension was immediately transferred to a centrifuge tube and spun at 1000 rpm for 3 min at RT. The supernatant was removed, the cell pellet was resuspended in 4 mL of culture medium, and the cell suspension was applied to a feeder-layer of SNL76/7 in a culture dish and cultured at 37°C, 5% CO_2. In the procedure, we carefully treated cells not to disperse into single cells, but to maintain cell clumps, because hiPS cells hardly proliferate when they were seeded as a single cell.

Cell colonies were observed under a phase contrast microscope after 1 day of culture. For a control experiment, hiPS cells without cryopreservation were seeded onto a SNL feeder-layer. To determine the recovery rates of hiPS cells after cryopreservation, cell colonies formed on the SNL cell layer were counted 1 day after culture. Recovery rates were calculated as follows:

Recovery rate (%) = 100 ×(the number of cell colonies formed by hiPS cells after preservation under liquid nitrogen) / (the number of cell colonies formed by hiPS cells without preservation).